Generation of EBV-transformed cell lines

EBV-transformed cell lines (EBV-LCLs) were generated by in vitro transformation of human B cells with EBV (strain B95-8), as described elsewhere (10). Based on the results of *STAT1* sequence analysis, EBV-LCLs from Patient 1 with T385M and wild-type (Wt) alleles and Patient 3 with R274Q and Wt alleles were designated as T385M/Wt and R274Q/Wt, respectively. Two age-matched control EBV-LCLs, designated Wt-1 and Wt-2, were used as controls. EBV-LCLs from Patient 2 were not obtained.

Stimulation reagents

For stimulation, 1:1000 diluted recombinant human IFN-γ 1a (Shionogi, Osaka, Japan; 1000 JRU/ml, 200 ng/ml), 1500 U/ml recombinant human IFN-α (Biosource International, Camarillo, CA), 20 ng/ml IL-27 (R&D Systems, Minneapolis, MN), and 100 μg/ml Curdlan (Wako, Osaka, Japan) were used.

DNA isolation, PCR, and sequence analysis of PCR products and TOPO-TA clones

These procedures were performed following the methods described elsewhere (10).

Measurement of CXCL10 (IP-10) concentration in supernatant of monocyte-derived macrophages and EBV-LCLs using Cytometric Bead Array

To accurately evaluate STAT1 function by studying supernatant IP-10 production from macrophages, monocytes were first purified from PBMCs with CD14 MicroBeads (Miltenyi Biotec, Bergisch Gladbach, Germany) to avoid contamination of other cells. A total of 5×10^5 cells/ml monocytes was then differentiated into macrophages by culturing for 7 d in RPMI 1640 containing 10% FBS in the presence of 5 ng/ml M-CSF (R&D Systems). To determine the effect of IFN-γ, differentiated macrophages in triplicate were not stimulated, were stimulated with 1 μg/ml LPS (Sigma, St Louis, MO), or were prestimulated with 1000 U/ml (200 ng/ml) IFN-γ (Shionogi) for 2 h and then stimulated with 1 μg/ml LPS for 24 h (IFN-γ–LPS stimulation), and supernatant was harvested for IP-10 measurement. For studying IP-10 production from EBV-LCLs, 1×10^6 cells/ml EBV-LCLs were cultured in the presence of 1000 U/ml IFN-γ for 6 h. The concentration of IP-10 in the supernatant was measured with Cytometric Bead Array (BD, San Diego, CA), following the manufacturer's instructions. Data from triplicate independent experiments are reported as the mean ± SD.

Preparation of nuclear extract

Nuclear extract was prepared essentially as described previously (11). Briefly, harvested cells were washed with Ca^{2+} and Mg^{2+}-free PBS and pelleted by centrifugation at 1500 × *g* for 5 min at 4°C. The resulting cell pellets were resuspended in cytoplasmic extract buffer (10 mM HEPES [pH 7.9], 10 mM KCl, 0.1 mM EDTA, 0.1 mM EGTA, 1 mM DTT, 1 mM Na_3VO_4, 1 mM NaF [pH 8]) with the addition of the recommended volume of dissolved protease inhibitor mixture tablets (Roche). After incubation on ice for 15 min, a 1:16 volume of 10% Nonidet P-40 was added. The suspension was vortexed and then centrifuged at 1500 × *g* for 5 min at 4°C. The pellets were washed again with cytoplasmic extract buffer without Nonidet P-40, resuspended with nuclear extract buffer (20 mM HEPES [pH 7.9], 400 mM NaCl, 1 mM EDTA, 1 mM EGTA, 1 mM DTT, 1 mM Na_3VO_4, 1 mM NaF [pH 8]) with the addition of protease inhibitor, and incubated at 4°C for 30 min. After centrifugation at maximum speed for 5 min at 4°C, the supernatant was saved as nuclear extract. Protein concentration was measured by Protein Assay (Bio-Rad, Hercules, CA).

Western blot analysis

After addition of SDS sample buffer, 10 μg nuclear extract was separated by 7.5% polyacrylamide gels and transferred to Immobilon-P Transfer Membranes (Millipore, Billerica, MA). Anti-lamin A Ab (BioLegend, San Diego, CA) was used as a loading control for nuclear extract. All of the primary Abs were used at the final concentration of 1 μg/ml. HRP-conjugated anti-mouse IgG secondary Abs (GE Healthcare, Buckinghamshire, U.K.) were used at 1:2000 dilution. The blots were then visualized by Pierce Western blotting Substrate (Thermo, Rockford, IL).

Studies of STAT1 phosphorylation state and staurosporine and pervanadate treatment of cells

We assessed dephosphorylation with the tyrosine kinase inhibitor staurosporine in EBV-LCLs. A total of 1×10^6 cells/ml EBV-LCLs was stimulated with IFN-γ for 30 min and then incubated with 1 μM staurosporine (Alomone Labs, Jerusalem, Israel) for 15, 30, or 60 min. The phosphatase inhibitor pervanadate was prepared by mixing 200 mM sodium orthovanadate (Wako, Osaka, Japan) and 100 mM H_2O_2 at a 2:1 ratio for 15 min at 22°C. EBV-LCLs were treated with pervanadate (0.8 mM orthovanadate and 0.2 mM H_2O_2) for 5 min and then stimulated with IFN-γ for 30 min. The nuclear extract from each condition was subjected to SDS-PAGE. The phosphorylation state of STAT1 was evaluated with anti-human STAT1 (pY701) Ab purchased from BD. The membrane was then stripped and reprobed with anti-human STAT1 (BD) and anti-lamin A (BioLegend) Abs.

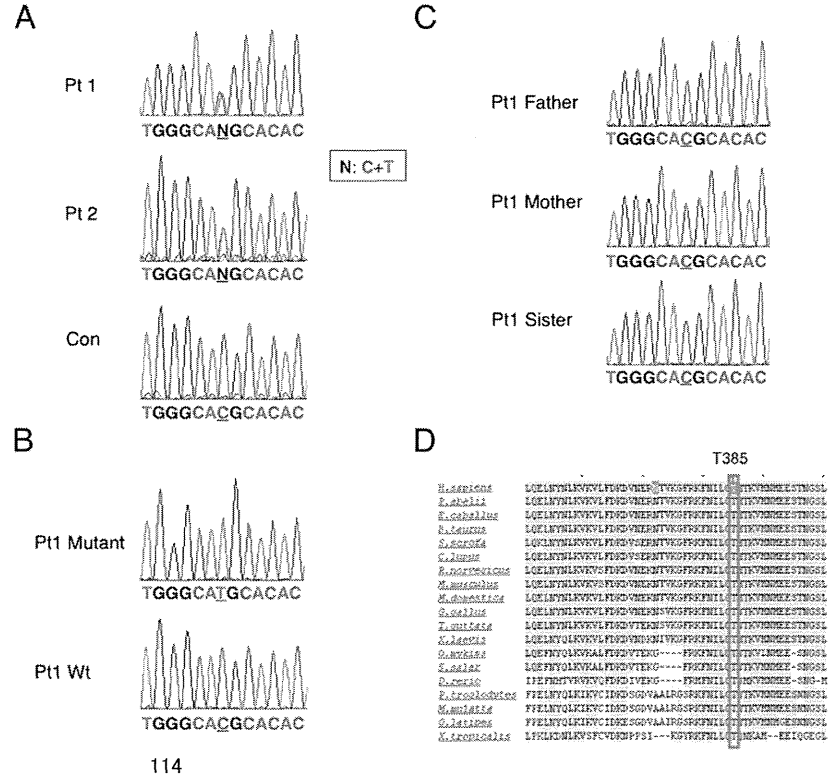

FIGURE 1. Patients 1 and 2 had the same heterozygous base change of c.1153C>T resulting in p.T385M in *STAT1*. (**A**) Direct sequence analysis of *STAT1* exon 14 in Patient 1 (Pt1) and Patient 2 (Pt2). Forward sequence is shown. (**B**) Sequence analysis of TOPO-TA clones of *STAT1* exon 14 PCR products in Patient 1. Mutant and Wt sequences are shown. (**C**) Direct sequence analysis of *STAT1* exon 14 in Patient 1's family members. (**D**) Comparison of the amino acid sequences of STAT1 in different species. The red box indicates the amino acids corresponding to p.T385 in humans. Con, Control.

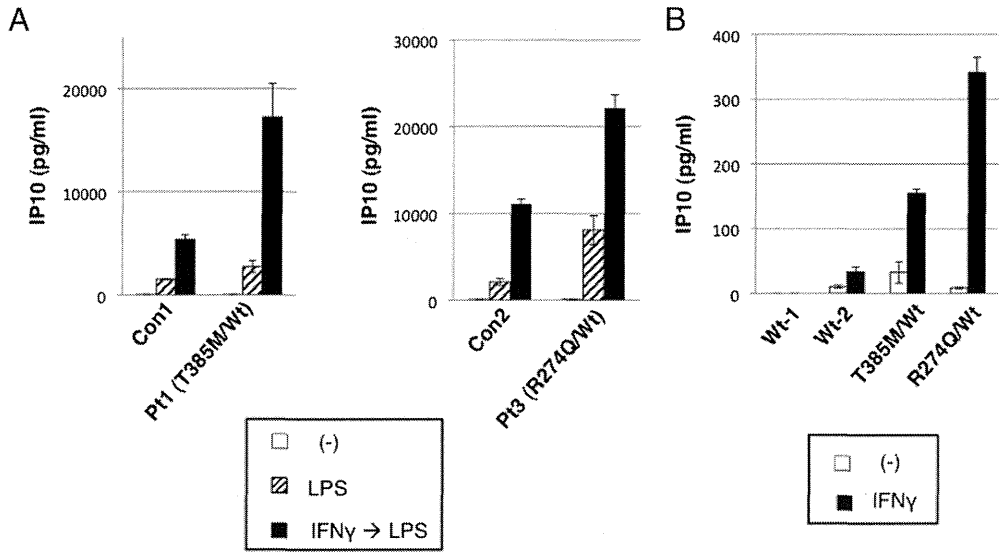

FIGURE 2. T385M was associated with higher levels of IP-10 production following IFN-γ stimulation in monocyte-derived macrophages and in EBV-LCLs. (**A**) Monocyte-derived macrophages were cultured in the presence of media, LPS, or IFN-γ–LPS for 24 h. IP-10 production was studied in the supernatant. Data shown are mean ± SD of triplicate independent experiments. (**B**) EBV-LCLs were stimulated with IFN-γ for 6 h, and IP-10 production was studied in the supernatant. Data shown are mean ± SD of triplicate independent experiments. Con1, Control for Patient 1 obtained and analyzed at the same time; Con2, control for Patient 3 obtained and analyzed at the same time; Pt1, Patient 1; Pt3, Patient 3; (−), media.

Flow cytometric analysis of intracellular IL-17A expression in CD4$^+$ cells

PBMCs at a density of 1 × 10^6 cells/ml were stimulated with 20 ng/ml PMA plus 500 ng/ml ionomycin for 6 h in the presence of GolgiStop (BD). Harvested PBMCs were washed and stained with PECy5-conjugated anti-human CD4 Ab (BioLegend) for 20 min at 4°C. Cells were washed three times and fixed and permeabilized with Cytofix/Cytoperm solution (BD) for 20 min at 4°C. Cells were then washed, incubated for 30 min with PE-conjugated anti-human IL-17A (BioLegend) or FITC-conjugated anti-human IFN-γ Abs (BioLegend), washed, and analyzed with a FACSCalibur (BD).

Results

A possible DBD mutation in STAT1

We first performed direct sequence analysis of the genes responsible for CMC in our patients: *AIRE*, *CLEC7A*, *CARD9*, *IL17RA*, *IL17F*, *IL2Rα*, and *STAT1* (4–6, 12–17). This study demonstrated that Patient 1 and Patient 2 have the same heterozygous base change in *STAT1* (c.1154C>T, p.T385M) (Fig. 1A), which was confirmed by the sequence analysis of TOPO-TA clones (Fig. 1B, data not shown). This base change has not been reported either as a mutation or as a single nucleotide polymorphism in the National Center for Biotechnology Information database, Ensembl database, or the Single Nucleotide Polymorphism Database, and it was not present in the family members of Patient 1 (Fig. 1C) or in 108 normal healthy controls (data not shown). Furthermore, the affected residue was evolutionarily conserved, as shown in Fig. 1D. The polymorphism phenotype-2 (PolyPhen-2) algorithm (http://genetics.bwh.harvard.edu/pph2/index.shtml), a structure sequence-based amino acid substitution-prediction method, predicted p.T385M as probably damaging, with a score of 1.000 (sensitivity: 0.00; specificity: 1.00). The sort intolerant from tolerant algorithm (http://sift.jcvi.org/) also predicted this amino acid substitution as deleterious. These results strongly indicate that c.1153C>T (p.T385M) is a de novo disease-causing mutation. Patient 1 was also shown to have an unreported heterozygous base change in *CARD9* (c.661G>A, p.K221E). However, this base change was also detected in his healthy father (data not shown). Additionally, PBMCs from Patient 1 showed normal IL-6 production in response

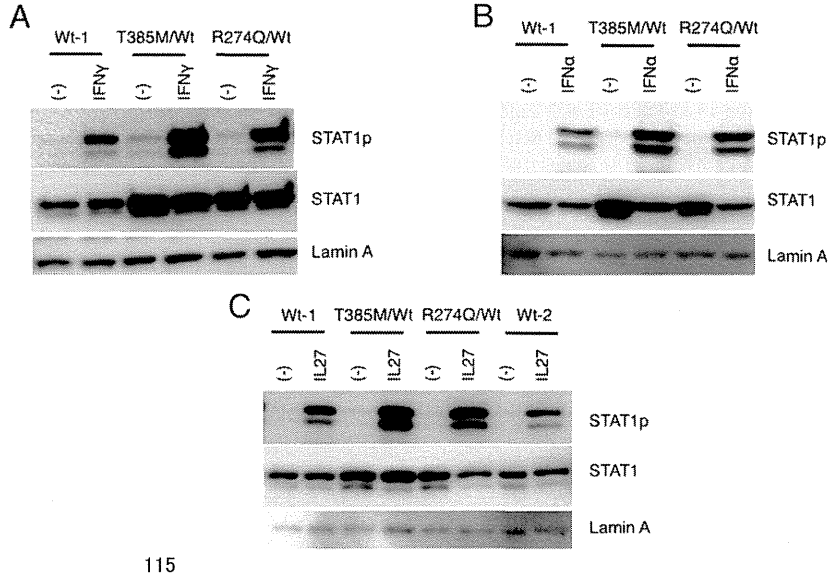

FIGURE 3. T385M was associated with hyperphosphorylation of STAT1 in response to IFN-γ, IFN-α, and IL-27 stimulation. Western blot analysis of STAT1p in nuclear extracts from EBV-LCLs was performed. Lamin A was used as a loading control. STAT1p expression in EBV-LCLs following IFN-γ (**A**), IFN-α (**B**), or IL-27 (**C**) stimulation for 30 min. (−), No stimulation.

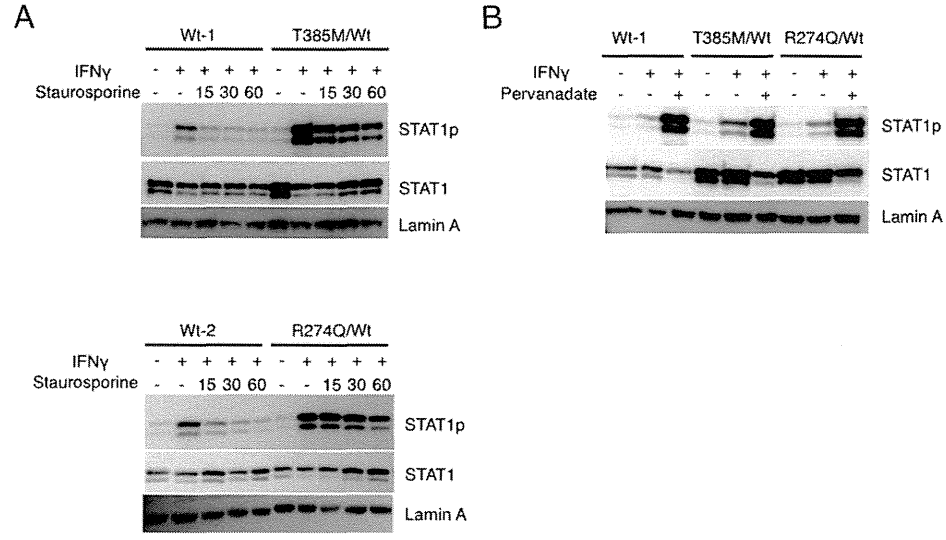

FIGURE 4. T385M was associated with hyperphosphorylation of STAT1 due to impaired dephosphorylation. (**A**) STAT1p expression in EBV-LCLs stimulated with IFN-γ for 30 min and then incubated with 1 μM staurosporine for 15, 30, or 60 min. (**B**) STAT1p expression in EBV-LCLs treated with pervanadate for 5 min and then stimulated with IFN-γ for 30 min.

to β-D-glucan stimulation with Curdlan (data not shown), indicating that the base change of c.661G>A, p.K221E in *CARD9* is not a disease-causing mutation but a single nucleotide polymorphism. The rest of the genes studied were demonstrated to be normal in both patients.

T385M is associated with gain of STAT1 function

Gain-of-function mutations in *STAT1* were very recently shown to be the genetic cause of autosomal-dominant or sporadic CMC (4–6). The reported mutations have been exclusively localized in the CC domain, leading to gain of STAT1 function due to impaired STAT1 dephosphorylation (4). To study whether the base change of c.1153C>T, p.T385M affecting the DBD of STAT1 also leads to gain of STAT1 function, the production of the downstream target of STAT1, IP-10, was studied following IFN-γ stimulation. IP-10 production was significantly higher in monocyte-derived macrophages from Patient 1 (T385M/Wt) and Patient 3 (R274Q/Wt) than in the matched control macrophages after IFN-γ–LPS stimulation (Fig. 2A). IP-10 production was also significantly higher in EBV-LCLs from Patient 1 (T385M/Wt) and Patient 3 (R274Q/Wt) after IFN-γ stimulation (Fig. 2B). These results indicated that T385M is a mutation leading to gain of STAT1 function.

STAT1 T385M leads to STAT1 hyperphosphorylation in response to IFN-γ, IFN-α, and IL-27 stimulation, which is due to impaired dephosphorylation

We then studied the STAT1 phosphorylation state in EBV-LCLs to determine the mechanisms of the gain of STAT1 function. Expression of phosphorylated STAT1 (STAT1p) protein following IFN-γ stimulation was higher in T385M/Wt and R274Q/Wt EBV-LCLs than in Wt EBV-LCLs (Fig. 3A). The hyperphosphorylated state of STAT1 was also observed following stimulation with IFN-α and IL-27 (Fig. 3B, 3C). Additionally, expression of total STAT1 in nuclear extract tends to be higher in T385M/Wt and R274Q/Wt EBV-LCLs than in Wt EBV-LCLs, especially without stimulation (Fig. 3). The mechanisms underlying STAT1 hyperphosphorylation in T385M/Wt EBV-LCLs were further explored with the tyrosine kinase inhibitor staurosporine and the phosphatase inhibitor pervanadate. The dephosphorylation of IFN-γ–ac-

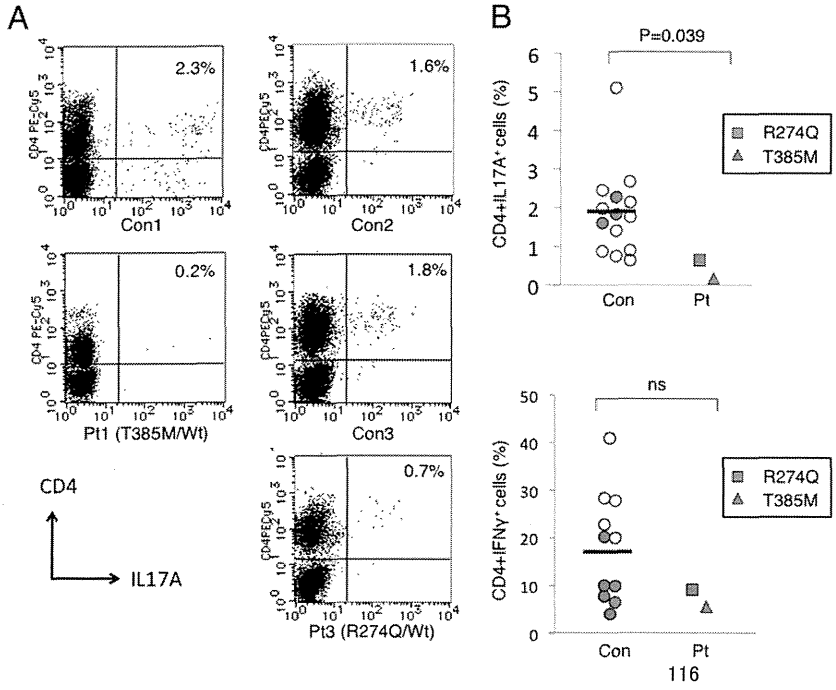

FIGURE 5. Patients 1 and 3 had deficient $CD4^+IL\text{-}17A^+$ cells but normal $CD4^+IFN\text{-}\gamma^+$ cells in response to PMA plus ionomycin stimulation. (**A**) Flow cytometric analysis of intracellular IL-17A expression following PMA plus ionomycin stimulation for 6 h. The proportion of $CD4^+IL\text{-}17A^+$ cells among $CD4^+$ cells was shown. (**B**) The proportion of $CD4^+IL\text{-}17A^+$ cells and $CD4^+IFN\text{-}\gamma^+$ cells among $CD4^+$ cells in normal controls and the patients. The horizontal lines indicate the mean proportion of $CD4^+IL\text{-}17A^+$ cells or $CD4^+IFN\text{-}\gamma^+$ cells in controls. Red and blue circles indicate controls obtained and analyzed at the same time as Patients 1 and 3, respectively. The *p* value was estimated using the Mann–Whitney *U* test. Con1, Control for Patient 1 obtained and analyzed at the same time; Con2 and Con3, controls for Patient 3 obtained and analyzed at the same time; Pt1, Patient 1; Pt3, Patient 3.

tivated T385M/Wt EBV-LCLs was impaired in the presence of staurosporine, as observed in R274Q/Wt EBV-LCLs (Fig. 4A). In contrast, with pervanadate treatment, the phosphorylation of STAT1 in T385M/Wt EBV-LCLs was similar to that seen in Wt EBV-LCLs (Fig. 4B). Therefore, the mechanisms underlying STAT1 hyperphosphorylation in T385M/Wt EBV-LCLs involve impaired dephosphorylation of STAT1, as observed in R274Q/Wt EBV-LCLs.

Patient 1 with the heterozygous T385M mutation in STAT1 had deficient Th17 cells

Deficient development of Th17 cells was documented to be associated with the development of CMC. CMC patients with gain-of-function mutations of *STAT1* affecting the CC domain have shown this defect (4). Therefore, we studied the proportion of $CD4^+IL\text{-}17A^+$ cells among $CD4^+$ cells in our patients after PMA plus ionomycin stimulation for 6 h. We also studied the population of $CD4^+IFN\text{-}\gamma^+$ cells to evaluate Th1 development. Patient 1 with the heterozygous T385M/Wt mutation of *STAT1* was reproducibly demonstrated to have dramatically reduced $CD4^+IL\text{-}17A^+$ cells (0.2% of $CD4^+$ cells), and Patient 3 with the heterozygous R274Q mutation had significantly reduced, but a little higher, $CD4^+IL\text{-}17A^+$ cells (0.7% of $CD4^+$ cells) (Fig. 5). The p value estimated using the Mann–Whitney U test was 0.039 between controls and the two patients. In contrast, both patients and controls had comparable percentages of $CD4^+IFN\text{-}\gamma^+$ cells (Fig. 5).

Discussion

To our knowledge, this study shows for the first time that the de novo heterozygous mutation of c.1153C>T in exon 14 (p.T385M), affecting the DBD of STAT1, is the genetic cause of sporadic CMC in two unrelated Japanese patients. The underlying mechanisms involve gain of STAT1 function due to impaired STAT1 dephosphorylation, as observed in the CC domain mutations (4).

Recent extensive studies of the STAT1 molecule reveal the association between the mutations affecting DBD and gain of STAT1 function. Based on crystallographic analysis, Darnell's group (7, 8) proposed a model of reorientation of phosphorylated "parallel" STAT1 dimers to an "antiparallel" form after leaving the DNA, which allows for reciprocal association of the CC domain and a pocket residue of the DBD for dephosphorylation. They further demonstrated in direct mutagenesis experiments that mutations of the pocket residues of the DBD, Q340A or Q340W, G384A or G384W, and Q408A or Q408W, resulted in impaired dephosphorylation of STAT1 (8). The fact that T385, the amino acid altered in two of our patients, is evolutionarily conserved and is positioned next to the pocket residue G384 may indicate that it is also critical in the reciprocal association with the CC domain for stabilizing the antiparallel structure and for dephosphorylation. It is also possible that this mutation of the DBD leads to impaired dissociation from the DNA, which may also cause a resistance to dephosphorylation of the STAT1 molecule. Higher expression of total STAT1 in nuclear extracts from T385M/Wt and R274Q/Wt EBV-LCLs than from Wt EBV-LCLs may reflect impaired nuclear export due to a resistance to dephosphorylation of the mutant STAT1 molecule (18), although the precise mechanisms were not determined in this study.

There may be more patients with CMC who carry gain-of-function mutations affecting the DBD of STAT1, given that significant numbers of patients with *STAT1* mutations are reported from all over the world (4–6). Additionally, crystallographic analysis and mutagenesis studies showed that mutations in the N-terminal domain (aa 1–130) also resulted in persistent phosphorylation (7, 8). This suggests that mutations affecting the N-terminal domain may also be a genetic cause of CMC.

We demonstrated deficient Th17 cells (0.2% of $CD4^+$ cells) in Patient 1 with the heterozygous T385M mutation, which was similar to or more severe than the defect observed in Patient 3 with the heterozygous R274Q mutation (0.7% of $CD4^+$ cells). Deficient development of Th17 cells may explain the increased susceptibility to *Candida* infection. IFN-γ, IFN-α, and IL-27 are potent inhibitors of Th17 cell development via STAT1 in mice and/or humans (19–21). Therefore, gain of STAT1 function in response to IFN-γ, IFN-α, or IL-27, which was observed in our patients, could be associated with deficient Th17 cell development. However, it remains to be determined precisely how gain of STAT1 function leads to deficient Th17 cells.

It is unclear whether there are differences in the clinical spectrum or severity of the disease between patients with the DBD mutations and the CC domain mutations. It might be worth noting that the two patients with the DBD mutation of T385M developed bronchiectasis in their early childhood, and one of them eventually developed HLH; these have not been described in patients with CC domain mutations.

With regard to HLH, administration of an anti–IFN-γ Ab was recently shown to have a therapeutic effect in two murine models of human hereditary HLH: perforin-deficient and Rab27a-deficient mice (22). Careful evaluation of the results indicates that T385M could be associated with higher expression of STAT1p in response to various stimulations (Fig. 3). Therefore, CMC patients with the DBD mutation of T385M may be more susceptible to the conditions presumably associated with enhanced IFN-γ–STAT1 signals, such as HLH. Detailed investigations of the clinical spectrum of these two populations should be conducted.

Acknowledgments

We thank Dr. D.M. Stewart (Metabolism Branch, National Cancer Institute, National Institutes of Health, Bethesda, MD) for reviewing the manuscript, the patients and their families for participation in this study, and Dr. H. Kanegane (Department of Pediatrics, Graduate School of Medicine, University of Toyama, Toyama, Japan) for coordinating patient recruitment.

Disclosures

The authors have no financial conflicts of interest.

References

1. Kirkpatrick, C. H. 1994. Chronic mucocutaneous candidiasis. *J. Am. Acad. Dermatol.* 31: S14–S17.
2. Mathis, D., and C. Benoist. 2009. Aire. *Annu. Rev. Immunol.* 27: 287–312.
3. Coleman, R., and R. J. Hay. 1997. Chronic mucocutaneous candidosis associated with hypothyroidism: a distinct syndrome? *Br. J. Dermatol.* 136: 24–29.
4. Liu, L., S. Okada, X. F. Kong, A. Y. Kreins, S. Cypowyj, A. Abhyankar, J. Toubiana, Y. Itan, M. Audry, P. Nitschke, et al. 2011. Gain-of-function human STAT1 mutations impair IL-17 immunity and underlie chronic mucocutaneous candidiasis. *J. Exp. Med.* 208: 1635–1648.
5. van de Veerdonk, F. L., T. S. Plantinga, A. Hoischen, S. P. Smeekens, L. A. Joosten, C. Gilissen, P. Arts, D. C. Rosentul, A. J. Carmichael, C. A. Smits-van der Graaf, et al. 2011. STAT1 mutations in autosomal dominant chronic mucocutaneous candidiasis. *N. Engl. J. Med.* 365: 54–61.
6. Smeekens, S. P., T. S. Plantinga, F. L. van de Veerdonk, B. Heinhuis, A. Hoischen, L. A. Joosten, P. D. Arkwright, A. Gennery, B. J. Kullberg, J. A. Veltman, et al. 2011. STAT1 hyperphosphorylation and defective IL12R/IL23R signaling underlie defective immunity in autosomal dominant chronic mucocutaneous candidiasis. *PLoS ONE* 6: e29248.
7. Zhong, M., M. A. Henriksen, K. Takeuchi, O. Schaefer, B. Liu, J. ten Hoeve, Z. Ren, X. Mao, X. Chen, K. Shuai, and J. E. Darnell, Jr. 2005. Implications of an antiparallel dimeric structure of nonphosphorylated STAT1 for the activation-inactivation cycle. *Proc. Natl. Acad. Sci. USA* 102: 3966–3971.
8. Mertens, C., M. Zhong, R. Krishnaraj, W. Zou, X. Chen, and J. E. Darnell, Jr. 2006. Dephosphorylation of phosphotyrosine on STAT1 dimers requires extensive spatial reorientation of the monomers facilitated by the N-terminal domain. *Genes Dev.* 20: 3372–3381.
9. Nagashima, T., A. Miyanoshita, Y. Sakiyama, Y. Ozaki, A. C. Stan, and K. Nagashima. 2000. Cerebral vasculitis in chronic mucocutaneous candidiasis: autopsy case report. *Neuropathology* 20: 309–314.

10. Yamada, M., Y. Okura, Y. Suzuki, S. Fukumura, T. Miyazaki, H. Ikeda, S. I. Takezaki, N. Kawamura, I. Kobayashi, and T. Ariga. 2012. Somatic mosaicism in two unrelated patients with X-linked chronic granulomatous disease characterized by the presence of a small population of normal cells. *Gene* 497: 110–115.
11. Schreiber, E., P. Matthias, M. M. Müller, and W. Schaffner. 1989. Rapid detection of octamer binding proteins with 'mini-extracts', prepared from a small number of cells. *Nucleic Acids Res.* 17: 6419.
12. Nagamine, K., P. Peterson, H. S. Scott, J. Kudoh, S. Minoshima, M. Heino, K. J. Krohn, M. D. Lalioti, P. E. Mullis, S. E. Antonarakis, et al. 1997. Positional cloning of the APECED gene. *Nat. Genet.* 17: 393–398.
13. Finnish-German APECED Consortium. 1997. An autoimmune disease, APECED, caused by mutations in a novel gene featuring two PHD-type zinc-finger domains. *Nat. Genet.* 17: 399–403.
14. Ferwerda, B., G. Ferwerda, T. S. Plantinga, J. A. Willment, A. B. van Spriel, H. Venselaar, C. C. Elbers, M. D. Johnson, A. Cambi, C. Huysamen, et al. 2009. Human dectin-1 deficiency and mucocutaneous fungal infections. *N. Engl. J. Med.* 361: 1760–1767.
15. Glocker, E. O., A. Hennigs, M. Nabavi, A. A. Schäffer, C. Woellner, U. Salzer, D. Pfeifer, H. Veelken, K. Warnatz, F. Tahami, et al. 2009. A homozygous CARD9 mutation in a family with susceptibility to fungal infections. *N. Engl. J. Med.* 361: 1727–1735.
16. Puel, A., S. Cypowyj, J. Bustamante, J. F. Wright, L. Liu, H. K. Lim, M. Migaud, L. Israel, M. Chrabieh, M. Audry, et al. 2011. Chronic mucocutaneous candidiasis in humans with inborn errors of interleukin-17 immunity. *Science* 332: 65–68.
17. Sharfe, N., H. K. Dadi, M. Shahar, and C. M. Roifman. 1997. Human immune disorder arising from mutation of the alpha chain of the interleukin-2 receptor. *Proc. Natl. Acad. Sci. USA* 94: 3168–3171.
18. McBride, K. M., C. McDonald, and N. C. Reich. 2000. Nuclear export signal located within theDNA-binding domain of the STAT1transcription factor. *EMBO J.* 19: 6196–6206.
19. Villarino, A. V., E. Gallo, and A. K. Abbas. 2010. STAT1-activating cytokines limit Th17 responses through both T-bet-dependent and -independent mechanisms. *J. Immunol.* 185: 6461–6471.
20. Ramgolam, V. S., Y. Sha, J. Jin, X. Zhang, and S. Markovic-Plese. 2009. IFN-beta inhibits human Th17 cell differentiation. *J. Immunol.* 183: 5418–5427.
21. Diveu, C., M. J. McGeachy, K. Boniface, J. S. Stumhofer, M. Sathe, B. Joyce-Shaikh, Y. Chen, C. M. Tato, T. K. McClanahan, R. de Waal Malefyt, et al. 2009. IL-27 blocks RORc expression to inhibit lineage commitment of Th17 cells. *J. Immunol.* 182: 5748–5756.
22. Pachlopnik Schmid, J., C. H. Ho, F. Chrétien, J. M. Lefebvre, G. Pivert, M. Kosco-Vilbois, W. Ferlin, F. Geissmann, A. Fischer, and G. de Saint Basile. 2009. Neutralization of IFNgamma defeats haemophagocytosis in LCMV-infected perforin- and Rab27a-deficient mice. *EMBO. Mol. Med.* 1: 112–124.

Severe Primary Antibody Deficiency Due to a Novel Mutation of μ Heavy Chain

I Mohammadzadeh,[1] M Yeganeh,[2] A Aghamohammadi,[3] N Parvaneh,[3] N Behniafard,[3] H Abolhassani,[3] F Tabassomi,[3] M Hemmat,[3] H Kanegane,[4] T Miyawaki,[4] O Ohara,[5] N Rezaei[3,6]

[1]*Department of Pediatrics, Amirkola Hospital, Babol University of Medical Sciences, Babol, Iran*

[2]*Division of Immunology, Department of Pediatrics, Faculty of Medicine, University of Sherbrooke, Centre de Recherche Clinique Etienne Le-Bel, Centre Hopitalier Universitaire de Sherbrooke, Sherbrooke, Canada*

[3]*Research Center for Immunodeficiencies, Children's Medical Center, Tehran University of Medical Sciences, Tehran, Iran*

[4]*Department of Pediatrics, Faculty of Medicine, Toyama Medical and Pharmaceutical University, Toyama, Japan*

[5]*Department of Human Genome Research, Kazusa DNA Research Institute, Chiba, Japan*

[6]*Molecular Immunology Research Center; and Department of Immunology, School of Medicine, Tehran University of Medical Sciences, Tehran, Iran*

Key words: Agammaglobulinemia. Antibody deficiency. B cell development. Mutation. Immunodeficiency. Infection.

Palabras clave: Agammaglobulinemia. Deficiencia de anticuerpos. Desarrollo de linfocitos B. Mutación. Inmunodeficiencia. Infección.

Primary antibody deficiencies are the most common primary immunodeficiency diseases in children [1]. A subset of patients are affected by the loss of genes implicated in the maturation of B cells in the bone marrow. Early development of B cells is characterized by maturation of the B cell receptor (BCR) and its downstream signaling pathways. BCR maturation includes 2 checkpoints, namely a pro-B-cell stage ($CD34^+CD10^+CD19^+$) and a pre-B-cell stage ($CD34^-CD10^+CD19^+$). During the pro-B-cell stage, different components of BCR are expressed onto the surface of B cells to create appropriate conditions for the pre-BCR stage. Intact pre-BCR signaling leads to the rearrangement of light chains and the expression of BCR on naïve B cells [2]. B cells migrate to secondary lymphoid organs for further adaptive maturation and eventually plasma cell and memory B-cell formation.

Bruton tyrosine kinase (BTK) plays a crucial role in the pre-BCR signaling pathway. *BTK* mutations are responsible for X-linked agammaglobulinemia (XLA), which is the prototype of early B-cell maturation disorders [3]. Other known causes in humans are autosomal recessive mutations of pre-BCR components (μ-heavy chain [μHC], CD79a, CD79b, λ5) and BLNK, which is a scaffold protein in pro-BCR signaling [4].

Both XLA and recessive forms of agammaglobulinemia share 3 diagnostic criteria: profoundly decreased levels of serum globulins, recurrent bacterial infections, and absence of circulating B cells. However, clinical course may vary and therefore mutation analysis is needed to clearly identify etiology. Here, we present the case of a patient with impaired early B-cell maturation and severe clinical presentation in whom we found a novel homozygous mutation in the gene coding for μHC.

A 20-year old man was referred due to a life-long history of recurrent infections. He was the second child of consanguineous parents and had an older sister and a younger brother, both healthy. There were no signs of immunodeficiency in any other members of the family. The patient was fully immunized at birth, and no complications were observed.

He remained well until the age of 3 months, when he developed frequent pneumonia episodes, requiring several outpatient admissions, followed by recurrent arthritis with hospitalization every other year. Due to the destruction of joints, he had an unusual gait. At 10 years of age, he lost his hearing due to severe recurrent otitis media. Unfortunately, there was no information about the causative pathogens. We also noticed growth retardation (below the third percentile for his age group), unilateral inguinal hernia, delayed pubertal development, and small-for-age genitalia. Moreover the clubbing of his fingers indicated a prolonged respiratory disorder, confirmed by spirometry.

The levels of all immunoglobulin isotypes were below normal: immunoglobulin (Ig) G=25 mg/dL (normal range, 656-1350 mg/dL), IgM=4 mg/dL (normal range,120-320 mg/dL), IgA=absent (normal range, 86-320 mg/dL), IgE=1 IU/L (normal range, 0-46 IU/L). Immunophenotyping of peripheral blood lymphocytes showed extensive reduction of B cells (<1% of total lymphocytes) with a normal T-cell population. At 3 years of age, the patient was put on prophylactic antibiotics and intramuscular immunoglobulin, which was switched to intravenous immunoglobulin (IVIg) at the age of 5 years. Unfortunately, he died due to septicemia and disseminated intravascular coagulation at the age of 20 years.

Western blot analysis disclosed normal BTK expression. Given the consanguinity of the parents, we sequenced known genes previously shown to be associated with a similar phenotype (see above), and found a novel homozygous mutation in the gene coding for μHC. A frame shift insertion in the first exon (c.525-526 ins. C) led to a premature stop codon in the CH2 domain.

Disorders with impaired antibody production can be categorized according to early or late B-cell maturation. Defects affecting early B-cell development are associated with a reduced number of circulating B cells, whereas in later stages, B cells are not able to efficiently produce antibodies. While our understanding of early B-cell maturation is relatively solid, much remains to be learned about later stages. In fact, most patients with defective antibody production belong to this second category. Although mutated genes involved in somatic hypermutation, class switch recombination, and germinal center formation have been implicated in a substantial number of patients [5, 6], we do not have a clear explanation yet.

Patients with defective early B-cell maturation in the bone marrow are usually treated with life-long monthly IVIg infusions. Indeed, the introduction of agammaglobulinemia by Bruton in 1952 and its successful management [7] was followed by a series of observations indicating the relative benefits of parenteral immunoglobulin [8].

We have reported on a rather complicated case of antibody deficiency. The patient was clinically diagnosed at

3 years of age and subsequently received adequate treatment (400 mg/month IVIg) with conventional therapy. Despite this, however, he did not survive beyond his twenties. It is notable that the first manifestations were seen at 3 months, which is a relatively young age compared to the situation in XLA patients [3]. Given that early diagnosis of antibody deficiencies can dramatically improve treatment outcomes [9], the patient might have been a victim of delayed diagnosis. He also had recurrent bacterial arthritis, which is not a usual presentation of XLA [3]. Most patients with XLA reach a normal life span with IVIg and prophylactic antibiotics. It has been suggested that XLA is a leaky form of B-cell maturation block when compared to autosomal recessive forms of the phenotype [2]. Therefore, delayed diagnosis in recessive forms of agammaglobulinemia might have more dramatic consequences.

The patient also had delayed secondary sexual growth and developmental anomalies. To the best of our knowledge, pure B-cell deficiencies have not been described as a syndromic disorder. However, given the fact that the patient's parents were consanguineous, it might be possible that he was affected by other mutated genes. We cannot rule out such a putative coincidence.

In conclusion, we have described a novel mutation in the gene coding the μHC compartment of BCR. Our case report endorses the face that pro-B arrests show a more severe presentation than XLA. B-cell biology at its very early development stages has still as many obscure corners as in later stages.

References

1. Yong PF, Chee R, Grimbacher B. Hypogammaglobulinaemia. Immunol Allergy Clin North Am. 2008;28:691-713.
2. Schiff C, Lemmers B, Deville A, Fougereau M, Meffre E Autosomal primary immunodeficiencies affecting human bone marrow B-cell differentiation. Immunol Rev. 2000;178:91-8.
3. Aghamohammadi A, Fiorini M, Moin M, Parvaneh N, Teimourian S, Yeganeh M, Goffi F, Kanegane H, Amirzargar AA, Pourpak Z, Rezaei N, Salavati A, Pouladi N, Abdollahzade S, Notarangelo LD, Miyawaki T, Plebani A. Clinical, immunological and molecular characteristics of 37 Iranian patients with X-linked agammaglobulinemia. Int Arch Allergy Immunol. 2006;141:408-14.
4. Conley ME, Dobbs AK, Farmer DM, Kilic S, Paris K, Grigoriadou S, Coustan-Smith E, Howard V, Campana D. Primary B cell immunodeficiencies: comparisons and contrasts. Annu Rev Immunol. 2009;27:199-227.
5. Kracker S, Gardes P, Mazerolles F, Durandy A. Immunoglobulin class switch recombination deficiencies. Clin Immunol. 2010;135:193-203.
6. Castigli E, Geha RS. Molecular basis of common variable immunodeficiency. J Allergy Clin Immunol. 2006;117:740-6.
7. Bruton OC. Agammaglobulinemia. Pediatrics 1952;9:722-8.
8. Dashti-Khavidaki S, Aghamohammadi A, Farshadi F, Movahedi M, Parvaneh N, Pouladi N, Moazzami K, Cheraghi T, Mahdaviani SA, Saghafi S, Heydari G, Abdollahzade S, Rezaei N. Adverse reactions of prophylactic intravenous immunoglobulin; a 13-year experience with 3004 infusions in Iranian patients with primary immunodeficiency diseases. J Investig Allergol Clin Immunol. 2009;19:139-45.
9. Aghamohammadi A, Pouladi N, Parvaneh N, Yeganeh M, Movahedi M, Gharagolou M, Pourpak Z, Rezaei N, Salavati A, Abdollahzade S, Moin M. Mortality and morbidity in common variable immunodeficiency. J Trop Pediatr. 2007;53:32-8.

Manuscript received March 12, 2011; accepted for publication, August 8, 2011.

Asghar Aghamohammadi
Research Center for Immunodeficiencies
Children's Medical Center Hospital
62 Qarib St, Keshavarz Blvd
Tehran 14194, Iran
E-mail: aghamohammadi@sina.tums.ac.ir

ERRATUM:

The title of the manuscript "High Prevalence of Asthma and Allergic Diseases in Children Aged 6 and 7 Years From the Canary Islands: The International Study of Asthma and Allergies in Childhood" published in Vol 19 n° 5 of JIACI should read as follows:

"High Prevalence of Asthma and Allergic Diseases in Children Aged 6 to 7 Years From the Canary Islands".
The running title should read "Allergy Prevalence in Canary Island Children"

Wnt3a stimulates maturation of impaired neutrophils developed from severe congenital neutropenia patient-derived pluripotent stem cells

Takafumi Hiramoto[a,b], Yasuhiro Ebihara[b,c,1], Yoko Mizoguchi[d], Kazuhiro Nakamura[d], Kiyoshi Yamaguchi[e], Kazuko Ueno[f], Naoki Nariai[f], Shinji Mochizuki[b,c], Shohei Yamamoto[b,c], Masao Nagasaki[f], Yoichi Furukawa[e], Kenzaburo Tani[a], Hiromitsu Nakauchi[g], Masao Kobayashi[d], and Kohichiro Tsuji[b,c]

[a]Division of Molecular and Clinical Genomics, Medical Institute of Bioregulation, Kyushu University, Higashi-ku, Fukuoka 812-8582, Japan; [c]Department of Pediatric Hematology/Oncology, Research Hospital, Divisions of [b]Stem Cell Processing and [g]Stem Cell Therapy, Center for Stem Cell Biology and Regenerative Medicine, and [e]Division of Clinical Genome Research, Advanced Clinical Research Center, Institute of Medical Science, University of Tokyo, Minato-ku, Tokyo 108-8639, Japan; [d]Pediatrics, Hiroshima University Graduate School of Biomedical and Health Sciences, Minami-ku, Hiroshima 734-8551, Japan; and [f]Department of Integrative Genomics, Tohoku Medical Megabank Organization, Tohoku University, Aramaki, Aoba-ku, Sendai 980-8573, Japan

Edited by George Q. Daley, Children's Hospital Boston, Boston, MA, and accepted by the Editorial Board January 4, 2013 (received for review October 1, 2012)

The derivation of induced pluripotent stem (iPS) cells from individuals of genetic disorders offers new opportunities for basic research into these diseases and the development of therapeutic compounds. Severe congenital neutropenia (SCN) is a serious disorder characterized by severe neutropenia at birth. SCN is associated with heterozygous mutations in the neutrophil elastase [elastase, neutrophil-expressed (ELANE)] gene, but the mechanisms that disrupt neutrophil development have not yet been clarified because of the current lack of an appropriate disease model. Here, we generated iPS cells from an individual with SCN (SCN-iPS cells). Granulopoiesis from SCN-iPS cells revealed neutrophil maturation arrest and little sensitivity to granulocyte-colony stimulating factor, reflecting a disease status of SCN. Molecular analysis of the granulopoiesis from the SCN-iPS cells vs. control iPS cells showed reduced expression of genes related to the wingless-type mmtv integration site family, member 3a (Wnt3a)/β-catenin pathway [e.g., lymphoid enhancer-binding factor 1], whereas Wnt3a administration induced elevation lymphoid enhancer-binding factor 1-expression and the maturation of SCN-iPS cell-derived neutrophils. These results indicate that SCN-iPS cells provide a useful disease model for SCN, and the activation of the Wnt3a/β-catenin pathway may offer a novel therapy for SCN with ELANE mutation.

apoptosis | unfolded protein response | SCN disease model

Severe congenital neutropenia (SCN) is a heterogeneous bone marrow (BM) failure syndrome characterized by severe neutropenia at birth, leading to recurrent infections by bacteria or fungi (1). SCN patients reveal an arrest in neutrophil differentiation in the BM at the promyelocyte or myelocyte stage (1), as well as a propensity to develop myelodysplastic syndrome and acute myeloid leukemia (2). Current treatment by high-dose granulocyte-colony stimulating factor (G-CSF) administration induces an increase in the number of mature neutrophils in the peripheral blood of most SCN patients (3). Although this treatment is curative for the severe infections, there is a concern that high-dose G-CSF may increase the risk of hematologic malignancy in these individuals (4).

Several genetic mutations have been identified in SCN patients. Approximately 50% of autosomal-dominant SCN cases were shown to have various heterozygous mutations in the gene encoding neutrophil elastase [elastase, neutrophil-expressed (ELANE)] (5, 6), a monomeric, 218-amino acid (25 kDa) chymotryptic serine protease (7) that is synthesized during the early stages of primary granule production in promyelocytes (8, 9). However, the mechanism(s) causing impaired neutrophil maturation in SCN patients remains unclear due to the current lack of an appropriate disease model.

Results and Discussion

In the present study, we generated induced pluripotent stem (iPS) cells from the BM cells obtained from an SCN patient with a heterologous ELANE gene mutation (exon 5, 707 region, C194X) (SCN-iPS cells) to provide the basis for an SCN disease model. The patient who donated BM cells recurrently suffered from severe infections without exogenous G-CSF administration, but the G-CSF administration once a week prevented his repeated infection. The SCN-iPS cells continued to show embryonic stem cell morphology after >20 passages and also expressed pluripotent markers (Fig. S1*A*). The silencing of exogenous genes and the capability to differentiate into three germ layers by teratoma formation were confirmed for each of the three SCN-iPS cell clones (Fig. S1 *B* and *C*). Furthermore, the same ELANE gene mutation that was present in the patient persisted in the SCN-iPS cells (Fig. S1*D*). The SCN-iPS cells, as well as control iPS cells that were generated from healthy donors, had the normal karyotype (Fig. S1*E*) (10, 11) and no mutations in the mutation-sensitive region of the G-CSF receptor gene (12).

We first compared the hematopoietic differentiation from SCN-iPS cells with that from control iPS cells that were generated from healthy donors. SCN-iPS and control iPS cells were cocultured with a 15-Gy-irradiated murine stromal cell line (the AGM-S3 cell line), as reported (13). After 12 d, the cocultured cells were harvested, and the $CD34^+$ cells separated from these cells (SCN-iPS–$CD34^+$ and control iPS–$CD34^+$ cells, respectively) were cultured in a hematopoietic colony assay by using a cytokine mixture (*Materials and Methods*). The number and size of the erythroid (E) and mixed-lineage (Mix) colonies derived from SCN-iPS–$CD34^+$ cells (1×10^4 cells) were nearly identical to those of the corresponding colonies derived from control iPS–$CD34^+$ cells (E colonies: SCN-iPS cells, 11.0 ± 3.0, and control iPS cells, 11.4 ± 3.9; Mix colonies: SCN-iPS cells, 25.1 ± 7.2, and control iPS cells, 17.4 ± 4.0) (Fig. 1 *B* and *C* and Fig. S2 *A* and *B*). However, the number of myeloid colonies derived from SCN-iPS–$CD34^+$ vs. control iPS–$CD34^+$ cells was significantly lower (SCN-iPS cells, 47.4 ± 19.5; control iPS cells, 127.8 ± 17.9; $P < 0.01$), and the size of the colonies was also smaller (Fig. 1 *A*

Author contributions: T.H., Y.E., K.Y., S.M., S.Y., Y.F., K. Tani, H.N., M.K., and K. Tsuji designed research; T.H., Y.M., K.N., and K.Y. performed research; T.H., Y.E., Y.M., K.N., K.Y., K.U., N.N., S.M., S.Y., M.N., and K. Tsuji analyzed data; and T.H., Y.E., and K. Tsuji wrote the paper.

The authors declare no conflict of interest.

This article is a PNAS Direct Submission. G.Q.D. is a guest editor invited by the Editorial Board.

[1]To whom correspondence should be addressed. E-mail: ebihara@ims.u-tokyo.ac.jp.

This article contains supporting information online at www.pnas.org/lookup/suppl/doi:10.1073/pnas.1217039110/-/DCSupplemental.

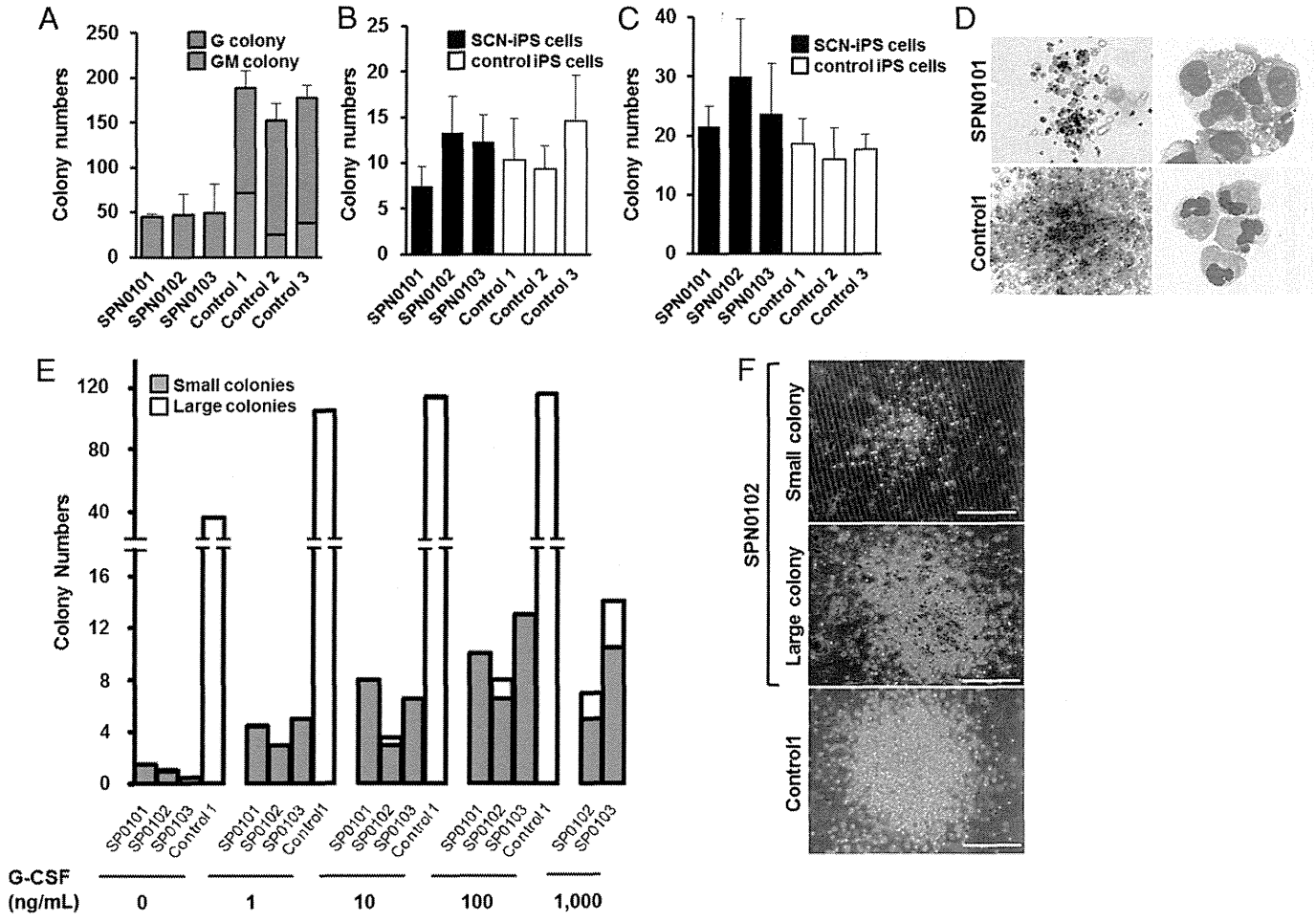

Fig. 1. Impaired neutrophil development from SCN-iPS cells. (*A*–C) A hematopoietic colony assay was performed by using 1×10^4 CD34$^+$ cells derived from three SCN-iPS cell clones (SPN0101, SPN0102, and SPN0103) and three control iPS cell clones (controls 1, 2, and 3) in the presence of a cytokine mixture. Colonies were sorted as myeloid (*A*), erythroid (*B*), and mixed-lineage (Mix) (*C*). Data are shown as mean ± SD. (*D*) Photographs of colonies (*Left*; 100×) and cells in a GM colony (*Right*; 400×; May–Grünwald–Giemsa staining). (*E*) A hematopoietic colony assay with dose escalation of G-CSF was performed by using 1×10^5 CD34$^+$ cells derived from SCN-iPS and control iPS cells. Filled and open bars indicate small colonies consisting of <100 cells and large colonies consisting of >100 cells, respectively. Data are shown as the average of three independent experiments. (*F*) Photographs of a small colony derived from SCN-iPS cells (SPN0102) in the presence of 10 ng/mL G-CSF, large colonies derived from SCN-iPS cells in the presence of 1,000 ng/mL G-CSF, and large colonies derived from control iPS cells (control 1) in the presence of 10 ng/mL G-CSF. (Scale bars, 200 μm.)

and *D*). In particular, only a few SCN-iPS cell-derived granulocyte (G) colonies—myeloid colonies consisting of only granulocytes—were detected (Fig. 1*A*). SCN-iPS cell-derived granulocyte–macrophage (GM) colonies—myeloid colonies consisting of macrophages/monocytes with/without granulocytes—contained a few immature myeloid cells in addition to macrophages/monocytes, whereas control iPS cell-derived GM colonies included a substantial number of mature, segmented, and band neutrophils (Fig. 1*D*).

We also found that Mix colonies derived from SCN-iPS cells, but not control iPS cells, contained immature myeloid cells and few mature neutrophils (Fig. S2 *C* and *D*). Next, we conducted a hematopoietic colony assay using various concentrations of G-CSF alone instead of the cytokine mixture to examine the G-CSF dose dependency of neutrophil differentiation from SCN-iPS and control iPS–CD34$^+$ cells. For all concentrations of G-CSF used (1–1,000 ng/mL), the SCN-iPS cell-derived myeloid colonies were significantly lower in number and smaller in size than the control iPS cell-derived myeloid colonies (Fig. 1*E*). Myeloid colony formation from control iPS cells reached a plateau at ~1–10 ng/mL G-CSF, whereas the number and size of those from SCN-iPS cells gradually increased with increasing concentrations of G-CSF. However, the values observed for SCN-iPS cells did not reach those for the control iPS cells, even at the highest dose of G-CSF used (1,000 ng/mL). Furthermore, large colonies consisting of >100 cells derived from SCN-iPS cells were only found with higher concentrations of G-CSF (Fig. 1*F*). Thus, granulopoiesis initiated from SCN-iPS cells was relatively insensitive to G-CSF, reflecting the inadequate in vivo response of neutrophils to G-CSF in SCN patients (14, 15). Therefore, these results support the applicability of the SCN-iPS cells established herein as a disease model for SCN.

To examine neutrophil development from SCN-iPS cells in more detail, SCN-iPS and control iPS–CD34$^+$ cells (1×10^4 cells each) were cocultured in suspension with AGM-S3 cells in the presence of neutrophil differentiation medium (*SI Materials and Methods*). The number of nonadherent cells derived from SCN-iPS–CD34$^+$ cells was lower than that from control iPS–CD34$^+$ cells on day 14 of culture (SCN-iPS cells, $9.77 \times 10^4 \pm 1.65 \times 10^4$ cells; control iPS cells, $52.48 \times 10^4 \pm 23.13 \times 10^4$ cells; $P < 0.05$) (Fig. 2*A*). The proportion of mature neutrophils among the nonadherent cells was also significantly lower for SCN-iPS cells relative to control iPS cells on day 14 (SPN-iPS cells, 15.53% ± 4.33%; control iPS cells, 71.285 ± 3.30%; $P < 0.05$) (Fig. 2 *B* and *C*), indicating that myeloid cells derived from SCN-iPS cells revealed the maturation arrest in the neutrophil development. We then examined a possibility that the maturation arrest in SCN-

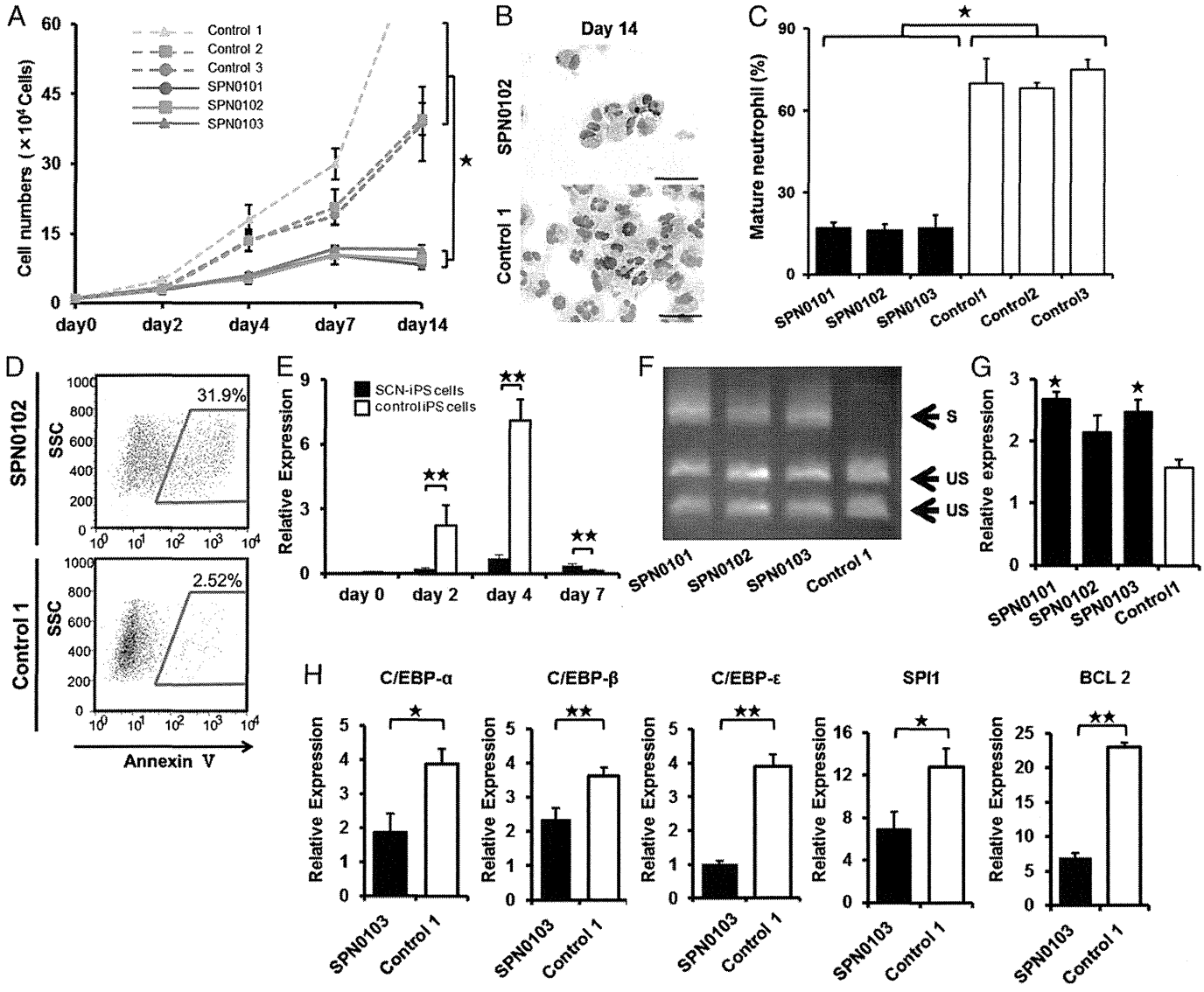

Fig. 2. Analysis of impaired neutrophil development from SCN-iPS cells. (*A*) Total number of nonadherent cells in the suspension culture of 1×10^4 $CD34^+$ cells derived from SCN-iPS and control iPS cells. Data are shown as mean ± SD. $^*P < 0.01$. (*B*) Photographs of nonadherent cells derived from SCN-iPS (SPN0103) and control iPS cells (control 1) on day 14 of culture (400×; May–Grünwald–Giemsa staining; scale bars, 50 μm.) (*C*) Filled and open bars show the proportion of mature neutrophils among the cells derived from SCN-iPS (filled bars) and control iPS (open bars) cells on day 14 of suspension culture. Data are shown as mean ± SD. $^*P < 0.05$. (*D*) Flow cytometric analysis of annexin V expression on cultured cells from SCN-iPS cells (SPN0102) or control iPS cells (control 1) on day 7. (*E*) Sequential qRT-PCR analysis of the relative expression of ELANE mRNA [ELANE/hypoxanthine–guanine phosphoribosyltransferase (HPRT) expression]. Data obtained from independent experiments using three SCN-iPS cell clones (SPN0101, SPN0102, and SPN0103) and three control iPS cell clones are shown as mean ± SD. $^{**}P < 0.01$. (*F* and *G*) $CD34^+$ cells derived from SCN-iPS or control iPS cells were cultured in neutrophil differentiation medium (see text). On day 7, nonadherent cells were collected and analyzed. (*F*) Representative gel showing spliced (S) and unspliced (US) XBP-1 bands on day 7. (*G*) qRT-PCR analysis of the relative mRNA expression (target/HPRT expression) of BiP on day 7. Data are shown as mean ± SD. $^*P < 0.05$; different from control 1). (*H*) qRT-PCR analysis of the relative mRNA expression (target / HPRT expression) of C/EBP-α, C/EBP-β, C/EBP-ε, SPI1, and BCL2 genes in non-adherent cells derived from SCN-iPS cells (filled bars, SPN0103) and control iPS cells (open bars, control 1) on day 2 of suspension culture. Data are shown as the mean ± the s.d. ($^{**}P < 0.01$, $^*P < 0.05$).

iPS cell-derived myeloid cells might be caused by their apoptosis. In flow cytometric analysis, SCN-iPS cell-derived myeloid cells contained a significantly higher proportion of annexin V-positive cells than control iPS-derived myeloid cells on day 7 of culture, suggesting that the maturation arrest in myeloid cells derived from SCN-iPS cells might be caused by their apoptosis (Fig. 2*D*).

We next examined ELANE mRNA expression levels in nonadherent cells derived from SCN-iPS vs. control iPS cells (Fig. 2*E*). ELANE expression was significantly lower in nonadherent cells derived from SCN-iPS vs. control iPS cells on days 2 and 4 of culture ($P < 0.01$), as reported (16, 17). However, the former was a little higher than the latter on day 7 ($P < 0.01$). This result may be explained by the existence of SCN-iPS cell-derived myeloid cells arrested at an early stage along the neutrophil differentiation pathway even on day 7 of culture. We also examined the expression of proteinase 3 and azurocidin, which comprise a family of closely related genes encoding neutrophil granule proteins along with ELANE, and found these genes were more highly expressed on day 4 (Fig. S3).

It has been reported that induction of the endoplasmic reticulum stress (ER) response and the unfolded protein response (UPR) has been advanced as a potential explanation for the molecular pathogenesis of SCN (18, 19). Thus, we examined activation of the UPR by X-box binding protein 1 (XBP-1) mRNA splicing on day 7. As shown in Fig. 2*F*, SPN-iPS cells induced XBP-1 mRNA splicing. We also found the up-regulation of BiP

(also known as GRP78 or HSPA5) (Fig. 2*G*). These results suggested that ER stress response and UPR might be involved in the pathogenesis in SCN.

To examine further the differences in gene expression between the two cell types, a microarray analysis was carried out by using $CD34^+$ cells derived from SCN-iPS and control iPS cells (three clones of each) in suspension culture on day 2. At this early time point, differences in cell number and morphology were not yet readily discernible between SCN-iPS and control iPS cells, as shown in Fig. 2*A*. However, the microarray analysis revealed a differential expression of various genes between the two cell types. Transcription factor genes, which were related to neutrophil development [e.g., CCAAT/enhancer-binding protein (C/EBP)-α (20), C/EBP-β (21), C/EBP-ε (22), and SPI1 (also known as PU.1) (23)], were all down-regulated in SCN-iPS cells. B-cell chronic lymphocytic leukemia/lymphoma 2, which regulates cell death under ER stress through the core mitochondrial apoptosis pathway (24), was also down-regulated (Fig. 3*A*). These findings were confirmed by quantitative reverse-transcriptional PCR (qRT-PCR), as shown in Fig. 2*H*.

Notably, the down-regulation of the genes in SCN-iPS cells related to and regulated by the wingless-type mmtv integration site family, member 3a (Wnt3a)/β-catenin pathway [e.g., Wnt3a, lymphoid enhance-binding factor (LEF)-1, BIRC5 (also known as survivin), and cyclin D1] was also uncovered by microarray analysis and qRT-PCR (Fig. 3 *A–C* and Fig. S4). Therefore, we examined the effect of enhancement of Wnt3a/β-catenin signaling by exogenous Wnt3a addition on the neutrophil development of $CD34^+$ cells derived from SCN-iPS and control iPS cells. Although Wnt3a did not stimulate the survival, proliferation, and differentiation of $CD34^+$ cells derived from both iPS cells in the absence of cytokines stimulating myelopoiesis including G-CSF, the addition of Wnt3a to the neutrophil differentiation medium induced a dose-dependent increase in the percentage of mature neutrophils among the cultured cells, as shown in Fig. 3 *D* and *E*. Furthermore, when Wnt3a was added concurrently with 1,000ng/mL G-CSF, the proportion of mature neutrophils increased more than it did with Wnt3a or 1,000 ng/mL G-CSF alone, reaching a value comparable with that observed for control iPS cells (Fig. 4 *A* and *B*).

The reduced expression of LEF-1 (as regulated by the Wnt3a/β-catenin pathway) reportedly plays a critical role in the defective maturation of neutrophils in SCN patients (25). Therefore, we next examined LEF-1 mRNA expression in SCN-iPS–$CD34^+$ cells cultured in the presence of Wnt3a, G-CSF (1,000 ng/mL), or both. Wnt3a and G-CSF both enhanced LEF-1 mRNA expression, but the most significant increase was observed in the presence of Wnt3a plus G-CSF. LEF-1 expression in SCN-iPS–$CD34^+$ cells in response to Wnt3a plus G-CSF was almost the same as that in control iPS–$CD34^+$ cells (Fig. 4*C*). These results substantiate the importance of LEF-1 in neutrophil development and the pathogenesis of SCN, as shown (25). Moreover the

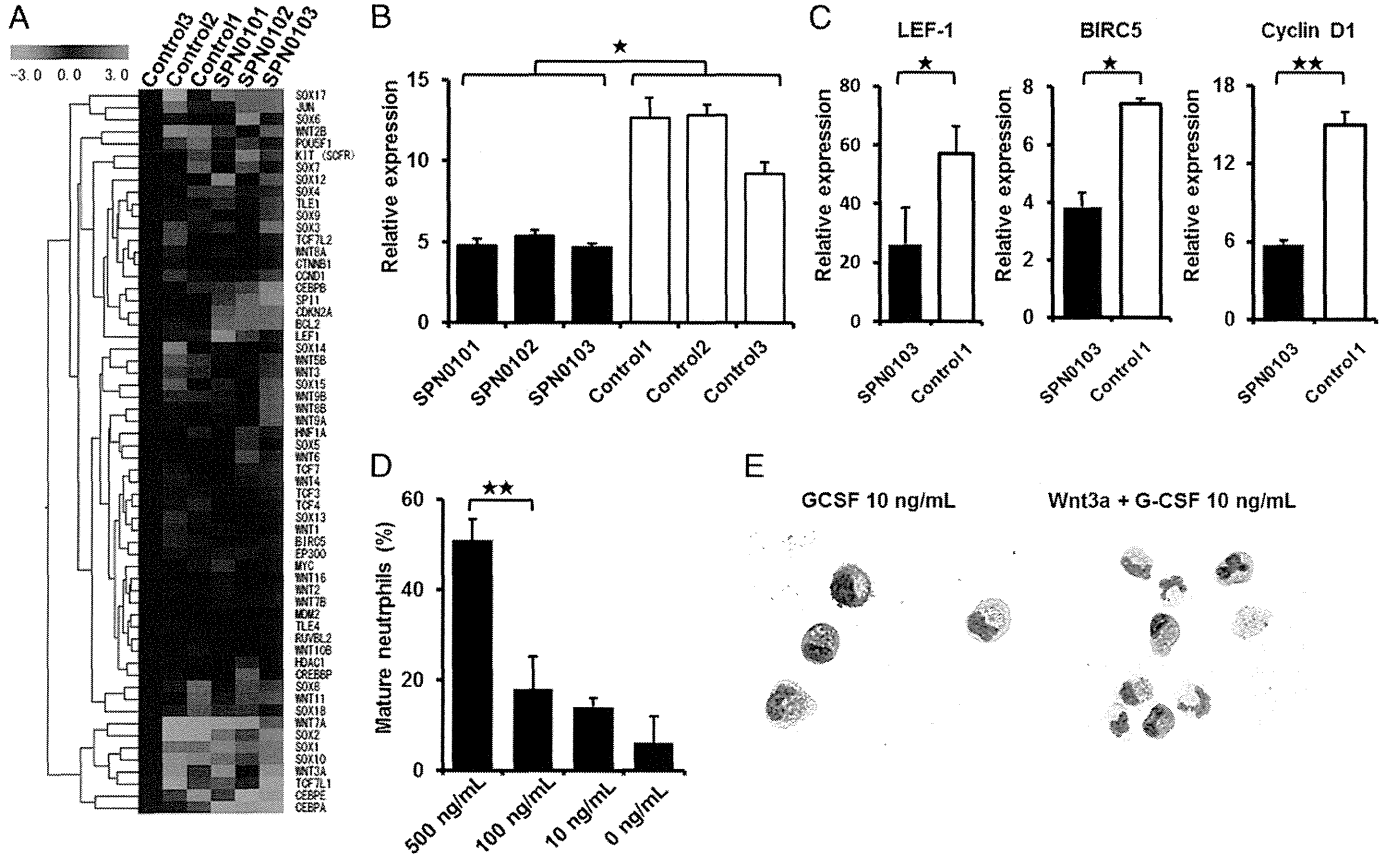

Fig. 3. Effects of Wnt3a on neutrophil development from SCN-iPS cells. (*A*) Heat map showing differential gene expression among SCN-iPS and control iPS cells on day 2. Red, high gene expression; blue, low gene expression compared with gene expression in control 3. (*B*) qRT-PCR analysis of the relative mRNA expression (target/HPRT expression) of Wnt3a on day 2. Filled and open bars indicate experiments using SCN-iPS cells (SPN0101, SPN0102, and SPN0103) and control iPS cells (controls 1, 2, and 3), respectively. Data are shown as mean ± SD. $^*P < 0.05$. (*C*) qRT-PCR analysis of the relative expression (target/HPRT expression) of genes regulated by the Wnt3a/β-catenin pathway (LEF-1, survivin, and cyclin D1) in SCN-iPS cells (filled bars, SPN0103) vs. control iPS cells (open bars, control 1) on day 2 of suspension culture. Data are shown as mean ± SD. $^{**}P < 0.01$; $^*P < 0.05$. (*D*) Proportion of mature neutrophils among the cells derived from SCN-iPS cells (SPN0102) on day 14 of suspension culture with dose escalation of Wnt3a. Data are shown as mean ± SD. $^{**}P < 0.01$. (*E*) Photographs of nonadherent cells on day 7 of suspension culture with or without Wnt3a (500 ng/mL) (400×; May–Grünwald–Giemsa staining).

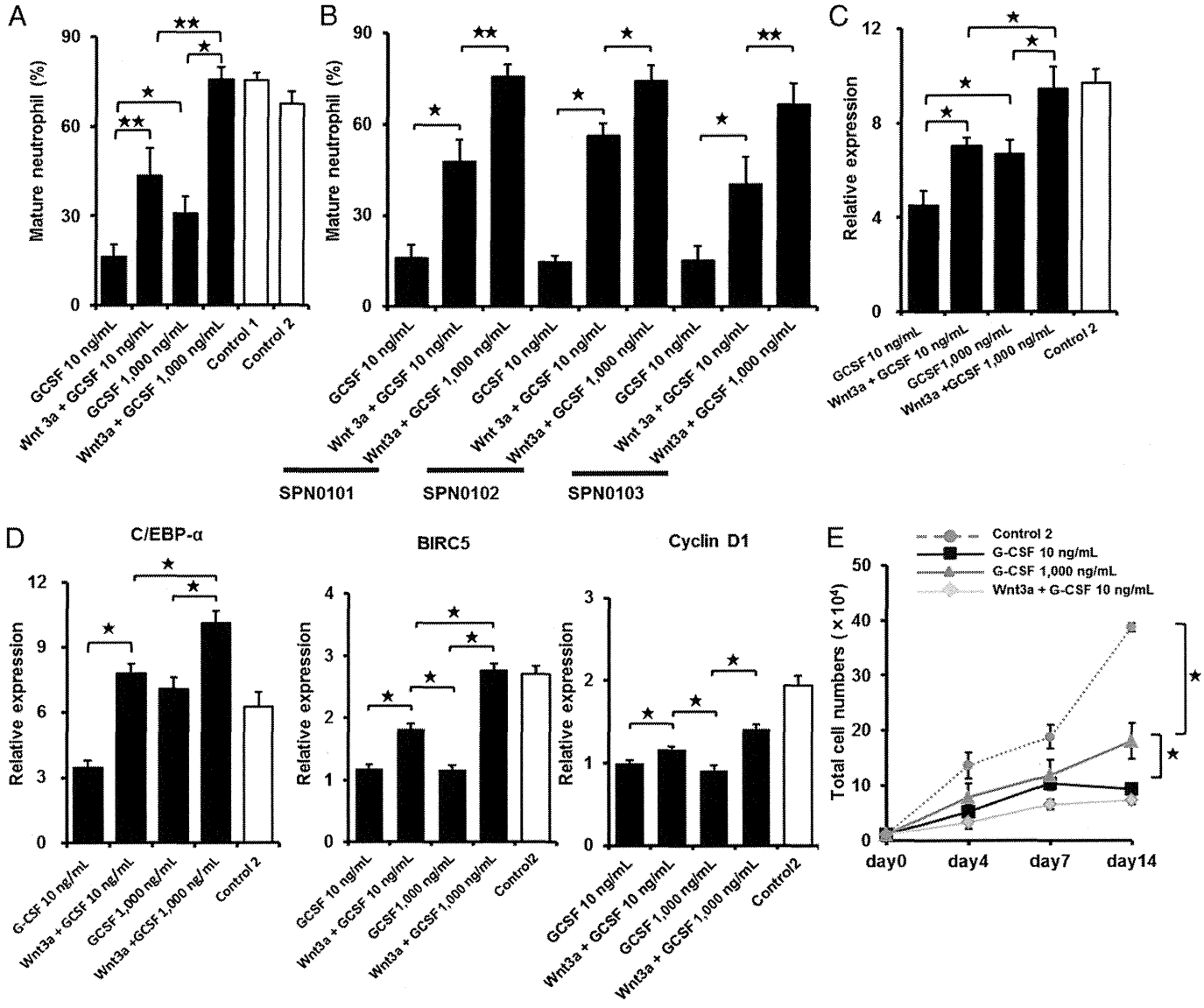

Fig. 4. Effects of Wnt3a in combination with high-dose G-CSF. (*A*) Filled and open bars show the proportion of mature neutrophils among the cells derived from SCN-iPS cells (SPN0101) on day 14 of suspension culture in the presence of neutrophil differentiation medium containing 10 ng/mL G-CSF (GCSF 10 ng/mL); 500 ng/mL Wnt3a and 10 ng/mL G-CSF (Wnt3a+GCSF 10 ng/mL); 1,000 ng/mL G-CSF (GCSF 1,000 ng/mL); or 500 ng/mL Wnt3a and 1,000 ng/mL G-CSF (Wnt3a + GCSF 1,000 ng/mL); and that from control iPS cells (controls 1 and 2) cultured in the neutrophil differentiation medium containing 10 ng/mL G-CSF, respectively. Data are shown as mean ± SD. $^{**}P < 0.01$; $^{*}P < 0.05$. (*B*) The proportion of mature neutrophils among the cells derived from three SCN-iPS cell clones (SPN0101, SPN0102, and SPN0103) on day 14 of suspension culture in the presence of neutrophil differentiation medium containing 10 ng/mL G-CSF (GCSF 10 ng/mL); 500 ng/mL Wnt3a and 10 ng/mL G-CSF (Wnt3a+GCSF 10 ng/mL); or 500 ng/mL Wnt3a and 1,000 ng/mL G-CSF (Wnt3a + GCSF 1,000 ng/mL). Data are shown as mean ± SD. $^{**}P < 0.01$; $^{*}P < 0.05$. (*C*) Filled and open bars show the relative expression (target/HPRT expression) of LEF-1 mRNA in SCN-iPS cells (SPN0101) on day 2 of suspension culture in the presence of differentiation medium containing the same combinations of Wnt3a and G-CSF as shown in *A* and that from control iPS cells (control 2), respectively. Data are shown as mean ± SD. $^{**}P < 0.01$; $^{*}P < 0.05$. (*D*) Filled and open bars show the relative expression (target/HPRT expression) of C/EBP-α, BIRC5, or cyclin D1 mRNA in SCN-iPS cells (SPN0101) on day 2 of suspension culture in the presence of differentiation medium containing the same combinations of Wnt3a and G-CSF as shown in *A* and that from control iPS cells (control 2), respectively. Data are shown as mean ± SD. $^{**}P < 0.01$; $^{*}P < 0.05$. (*E*) Total cell numbers of nonadherent cells in suspension cultures of 1×10^4 $CD34^+$ cells derived from control iPS cells (control 2; red broken line) and SCN-iPS cells (SPN0101) in the presence of neutrophil differentiation medium (black line) and those from SCN-iPS cells in the presence of neutrophil differentiation medium containing 500 ng/mL Wnt3a (yellow line) or 1,000 ng/mL G-CSF (black line). Data are shown as mean ± SD. $^{**}P < 0.05$.

administration of Wnt3a led to up-regulate C/EBP-α, cyclin D1, and BIRC5/survivin in addition to LEF-1 in the presence of G-CSF (Fig. 4*D*). These results suggested that the up-regulation of LEF-1 expression might promote granulopoiesis by increasing the expressions of cyclin D1, BIRC5/survivin, and C/EBP-α and its binding to LEF-1 in accordance with the previous report (25). Interestingly, Wnt3a did not stimulate the proliferation of myeloid cells, whereas 1,000 ng/mL G-CSF did to a certain extent (Fig. 4*E*). Hence, Wnt3a was capable of stimulating the maturation of impaired neutrophils in the presence of G-CSF, but not the proliferation of myeloid cells from SCN-iPS cells.

Importantly, aside from providing new insights into the mechanisms behind impaired neutrophil development in SCN patients, the present study demonstrates that agents activating the Wnt3a/β-catenin pathway are potential candidates for new drugs for SCN with mutations in the ELANE gene. Because endogenous G-CSF is readily increased in SCN patients (26), these activating agents may be viable alternatives to exogenous G-CSF treatment.

Materials and Methods

Additional information is available in *SI Materials and Methods*.

Generation of Human iPS Cells. BM fibroblasts from a patient with SCN and skin dermal fibroblasts from a healthy donor were acquired after obtaining informed consent after getting the approval by the Ethics Committee of the Institute of Medical Science, University of Tokyo, in accordance with the Declaration of Helsinki. The SCN patient presented with a heterozygous mutation in the ELANE gene in the 707 region of exon 5. SCN-iPS cells were established from the SCN-BM fibroblasts by transfection with the pMX retroviral vector, as described (10). This vector expressed the human transcription factors OCT3/4, SOX2, KLF4, and c-MYC. Control iPS cell clones, control 1 (TkDN4-M) and control 3 (201B7), were gifts from K. Eto and S. Yamanaka (Kyoto University, Kyoto), respectively (10, 11). Control 2 (SPH0101) was newly generated from another healthy donor's skin dermal fibroblasts by using the same methods.

Hematopoietic Colony Assay. A hematopoietic colony assay was performed in an aliquot of culture mixture, which contained 1.2% methylcellulose (Shin-Etsu Chemical), 30% (vol/vol) FBS, 1% (vol/vol) deionized fraction V BSA, 0.1 mM 2-mercaptoethanol (2-ME), α-minimum essential medium, and a cytokine mixture consisting of 100 ng/mL human stem cell factor (hSCF) (Wako), 100 ng/mL fusion protein 6 [FP6; a fusion protein of interleukin (IL)-6 and IL-6 receptor] (a gift from Tosoh), 10 ng/mL human IL-3 (hIL-3) (a gift from Kirin Brewery), 10 ng/mL human thrombopoietin (hTPO) (a gift from Kirin Brewery), 10 ng/mL human G-CSF (a gift from Chugai Pharmaceutical), and 5 U/mL human erythropoietin (a gift from Kirin Brewery). For dose escalation experiments, various concentrations (0, 1, 10, 100, and 1,000 ng/mL) of G-CSF were used instead of the cytokine mixture described above. Colony types were determined according to established criteria on day 14 of culture by in situ observations under an inverted microscope (IX70; Olympus) (27).

Suspension Culture and Neutrophil Differentiation Assay. $CD34^+$ cells (1×10^4 cells) were cocultured with irradiate confluent AGM-S3 cells in neutrophil differentiation medium containing Iscove's modified Dulbecco's medium, 10% FBS, 3 mM L-glutamine, 1×10^{-4} M 2-ME, 1×10^{-4} M nonessential amino acids solution, 100 ng/mL hSCF, 100 ng/mL FP6, 10 ng/mL hIL-3, 10 ng/mL hTPO, and 10 or 1,000 ng/mL human G-CSF. Wnt3a (10, 100, or 500 ng/mL) (R&D) was then added. The medium was replaced with an equivalent volume of fresh medium every 4 d. Living, nonadherent cells were counted following 0.4% trypan blue staining.

PCR primer. All primer sets used in this study are shown in Table S1.

Statistical Analysis. All data are presented as mean ± SD. $P < 0.05$ was considered significant. Statistical analyses were performed by using Prism software (GraphPad).

ACKNOWLEDGMENTS. We thank the individual with SCN who participated in this study; K. Eto for providing control iPS cells (control 1; TkDN4-M); S. Yamanaka for providing control iPS cells (control 3; 206B7); and E. Matsuzaka and S. Hanada for technical assistance. This work was supported by in part by Ministry of Education, Culture, Sports, Science, and Technology of Japan (MEXT) Grants-in-Aid (to Y.E.) and Project for Realization of Regenerative Medicine (MEXT) Grants-in-Aid (to K.Tsuji).

1. Zeidler C, Germeshausen M, Klein C, Welte K (2009) Clinical implications of *ELA2-, HAX1-*, and G-CSF-receptor (*CSF3R*) mutations in severe congenital neutropenia. *Br J Haematol* 144(4):459–467.
2. Freedman MH, et al. (2000) Myelodysplasia syndrome and acute myeloid leukemia in patients with congenital neutropenia receiving G-CSF therapy. *Blood* 96(2):429–436.
3. Dale DC, et al. (1993) A randomized controlled phase III trial of recombinant human granulocyte colony-stimulating factor (filgrastim) for treatment of severe chronic neutropenia. *Blood* 81(10):2496–2502.
4. Rosenberg PS, et al.; Severe Chronic Neutropenia International Registry (2006) The incidence of leukemia and mortality from sepsis in patients with severe congenital neutropenia receiving long-term G-CSF therapy. *Blood* 107(12):4628–4635.
5. Xia J, et al. (2009) Prevalence of mutations in ELANE, GFI1, HAX1, SBDS, WAS and G6PC3 in patients with severe congenital neutropenia. *Br J Haematol* 147(4):535–542.
6. Horwitz MS, et al. (2007) Neutrophil elastase in cyclic and severe congenital neutropenia. *Blood* 109(5):1817–1824.
7. Hajjar E, Broemstrup T, Kantari C, Witko-Sarsat V, Reuter N (2010) Structures of human proteinase 3 and neutrophil elastase—so similar yet so different. *FEBS J* 277(10): 2238–2254.
8. Fouret P, et al. (1989) Expression of the neutrophil elastase gene during human bone marrow cell differentiation. *J Exp Med* 169(3):833–845.
9. Pham CT (2006) Neutrophil serine proteases: Specific regulators of inflammation. *Nat Rev Immunol* 6(7):541–550.
10. Takayama N, et al. (2010) Transient activation of c-MYC expression is critical for efficient platelet generation from human induced pluripotent stem cells. *J Exp Med* 207(13):2817–2830.
11. Takahashi K, et al. (2007) Induction of pluripotent stem cells from adult human fibroblasts by defined factors. *Cell* 131(5):861–872.
12. Germeshausen M, Ballmaier M, Welte K (2007) Incidence of CSF3R mutations in severe congenital neutropenia and relevance for leukemogenesis: Results of a long-term survey. *Blood* 109(1):93–99.
13. Ma F, et al. (2007) Novel method for efficient production of multipotential hematopoietic progenitors from human embryonic stem cells. *Int J Hematol* 85(5):371–379.
14. Konishi N, et al. (1999) Defective proliferation of primitive myeloid progenitor cells in patients with severe congenital neutropenia. *Blood* 94(12):4077–4083.
15. Nakamura K, et al. (2000) Abnormalities of primitive myeloid progenitor cells expressing granulocyte colony-stimulating factor receptor in patients with severe congenital neutropenia. *Blood* 96(13):4366–4369.
16. Skokowa J, Fobiwe JP, Dan L, Thakur BK, Welte K (2009) Neutrophil elastase is severely down-regulated in severe congenital neutropenia independent of ELA2 or HAX1 mutations but dependent on LEF-1. *Blood* 114(14):3044–3051.
17. Kawaguchi H, et al. (2003) Dysregulation of transcriptions in primary granule constituents during myeloid proliferation and differentiation in patients with severe congenital neutropenia. *J Leukoc Biol* 73(2):225–234.
18. Köllner I, et al. (2006) Mutations in neutrophil elastase causing congenital neutropenia lead to cytoplasmic protein accumulation and induction of the unfolded protein response. *Blood* 108(2):493–500.
19. Grenda DS, et al. (2007) Mutations of the ELA2 gene found in patients with severe congenital neutropenia induce the unfolded protein response and cellular apoptosis. *Blood* 110(13):4179–4187.
20. Pabst T, et al. (2001) AML1-ETO downregulates the granulocytic differentiation factor C/EBPalpha in t(8;21) myeloid leukemia. *Nat Med* 7(4):444–451.
21. Hirai H, et al. (2006) C/EBPbeta is required for 'emergency' granulopoiesis. *Nat Immunol* 7(7):732–739.
22. Bedi R, Du J, Sharma AK, Gomes I, Ackerman SJ (2009) Human C/EBP-ε activator and repressor isoforms differentially reprogram myeloid lineage commitment and differentiation. *Blood* 113(2):317–327.
23. Friedman AD (2007) Transcriptional control of granulocyte and monocyte development. *Oncogene* 26(47):6816–6828.
24. Hetz C (2012) The unfolded protein response: Controlling cell fate decisions under ER stress and beyond. *Nat Rev Mol Cell Biol* 13(2):89–102.
25. Skokowa J, et al. (2006) LEF-1 is crucial for neutrophil granulocytopoiesis and its expression is severely reduced in congenital neutropenia. *Nat Med* 12(10):1191–1197.
26. Mempel K, Pietsch T, Menzel T, Zeidler C, Welte K (1991) Increased serum levels of granulocyte colony-stimulating factor in patients with severe congenital neutropenia. *Blood* 77(9):1919–1922.
27. Nakahata T, Ogawa M (1982) Hemopoietic colony-forming cells in umbilical cord blood with extensive capability to generate mono- and multipotential hemopoietic progenitors. *J Clin Invest* 70(6):1324–1328.

blood

2012 119: 5458-5466
Prepublished online April 19, 2012;
doi:10.1182/blood-2011-05-354167

Frequent somatic mosaicism of *NEMO* in T cells of patients with X-linked anhidrotic ectodermal dysplasia with immunodeficiency

Tomoki Kawai, Ryuta Nishikomori, Kazushi Izawa, Yuuki Murata, Naoko Tanaka, Hidemasa Sakai, Megumu Saito, Takahiro Yasumi, Yuki Takaoka, Tatsutoshi Nakahata, Tomoyuki Mizukami, Hiroyuki Nunoi, Yuki Kiyohara, Atsushi Yoden, Takuji Murata, Shinya Sasaki, Etsuro Ito, Hiroshi Akutagawa, Toshinao Kawai, Chihaya Imai, Satoshi Okada, Masao Kobayashi and Toshio Heike

Blood (print ISSN 0006-4971, online ISSN 1528-0020), is published weekly by the American Society of Hematology, 2021 L St, NW, Suite 900, Washington DC 20036.

Frequent somatic mosaicism of *NEMO* in T cells of patients with X-linked anhidrotic ectodermal dysplasia with immunodeficiency

Tomoki Kawai,[1] Ryuta Nishikomori,[1] Kazushi Izawa,[1] Yuuki Murata,[1] Naoko Tanaka,[1] Hidemasa Sakai,[1] Megumu Saito,[2] Takahiro Yasumi,[1] Yuki Takaoka,[1] Tatsutoshi Nakahata,[2] Tomoyuki Mizukami,[3] Hiroyuki Nunoi,[3] Yuki Kiyohara,[4] Atsushi Yoden,[5] Takuji Murata,[5] Shinya Sasaki,[6] Etsuro Ito,[6] Hiroshi Akutagawa,[7] Toshinao Kawai,[8] Chihaya Imai,[9] Satoshi Okada,[10] Masao Kobayashi,[10] and Toshio Heike[1]

[1]Department of Pediatrics, Kyoto University Graduate School of Medicine, Kyoto, Japan; [2]Clinical Application Department, Center for iPS Cell Research and Application, Institute for Integrated Cell-Material Sciences, Kyoto University, Kyoto, Japan; [3]Division of Pediatrics, Department of Reproductive and Developmental Medicine, Faculty of Medicine, University of Miyazaki, Miyazaki, Japan; [4]Department of Pediatrics, Faculty of Medicine, Osaka University, Suita, Japan; [5]Department of Pediatrics, Osaka Medical College, Takatsuki, Japan; [6]Department of Pediatrics, Hirosaki University Graduate School of Medicine, Hirosaki, Japan; [7]Department of Pediatrics, Kishiwada City Hospital, Kishiwada, Japan; [8]Department of Human Genetics, National Center for Child Health and Development, Tokyo, Japan; [9]Department of Pediatrics, Niigata University, Niigata, Japan; and [10]Department of Pediatrics, Hiroshima University Graduate School of Biomedical Sciences, Hiroshima, Japan

Somatic mosaicism has been described in several primary immunodeficiency diseases and causes modified phenotypes in affected patients. X-linked anhidrotic ectodermal dysplasia with immunodeficiency (XL-EDA-ID) is caused by hypomorphic mutations in the *NF-κB essential modulator (NEMO)* gene and manifests clinically in various ways. We have previously reported a case of XL-EDA-ID with somatic mosaicism caused by a duplication mutation of the *NEMO* gene, but the frequency of somatic mosaicism of *NEMO* and its clinical impact on XL-EDA-ID is not fully understood. In this study, somatic mosaicism of *NEMO* was evaluated in XL-EDA-ID patients in Japan. Cells expressing wild-type NEMO, most of which were derived from the T-cell lineage, were detected in 9 of 10 XL-EDA-ID patients. These data indicate that the frequency of somatic mosaicism of *NEMO* is high in XL-ED-ID patients and that the presence of somatic mosaicism of *NEMO* could have an impact on the diagnosis and treatment of XL-ED-ID patients. (*Blood*. 2012;119(23):5458-5466)

Introduction

X-linked anhidrotic ectodermal dysplasia with immunodeficiency (XL-EDA-ID) is a disease with clinical features including hypohidrosis, delayed eruption of teeth, coarse hair, and immunodeficiency associated with frequent bacterial infections.[1-5] The gene responsible for XL-EDA-ID has been identified as *NF-κB essential modulator (NEMO)*.[6-8] NEMO is necessary for the function of IκB kinase, which phosphorylates and degrades IκB to activate NF-κB.[9-10] Defects in NEMO cause various abnormalities in signal transduction pathways involving NF-κB, and affect factors such as the IL-1 family protein receptors, the TLRs, VEGFR-3, receptor activator of nuclear factor κB (RANK), the ectodysplasin-A receptor, CD40, and the TNF receptor I.[7] Whereas a complete loss of NEMO function in humans is believed to cause embryonic lethality,[11] *NEMO* mutations in XL-EDA-ID patients are hypomorphic,[8] causing a partial loss of NEMO functions.

In XL-EDA-ID, NEMO defects lead to diverse immunologic features including susceptibility to pathogens, impaired Ab response to polysaccharides,[2,4,12] hypogammaglobulinemia,[13] hyper IgM syndrome,[14] and impaired NK-cell activity,[15] with a large degree of variability in phenotypes among the patients. For example, approximately one-tenth of XL-EDA-ID patients exhibit reduced mitogen-induced proliferation of T lymphocytes.[12] Moreover, one-fourth suffer from inflammatory disorders such as inflammatory bowel disease and rheumatoid arthritis,[12] although the inflammatory process usually relies on NF-κB activation.[16] One explanation for this clinical variability is that the XL-EDA-ID phenotype is *NEMO* genotype-specific. Although the XL-EDA-ID database reported by Hanson et al succeeds to some extent in linking the specific clinical features to *NEMO* genotype,[12] the penetrance of some clinical features is not high and the mechanism accounting for this variability is unknown.

Recently, we have reported a case of spontaneous reversion mosaicism of the *NEMO* gene in XL-EDA-ID, which showed an atypical phenotype involving decreased mitogen-induced T-cell proliferation along with decreased CD4 T cells (patient 1).[17] There have been no subsequent reports on somatic mosaicism in XL-EDA-ID, and its prevalence and impact on the clinical features of the disease is unknown. In this study, we describe the younger brother of patient 1, who suffered from XL-EDA-ID with the same mutation and somatic reversion mosaicism of *NEMO*. Patient 2 showed intriguing laboratory findings in that mitogen-induced T-cell proliferation varied in accordance with the rate of detected reversion in the peripheral blood. These 2 cases led us to perform a nationwide study of XL-EDA-ID patients in Japan that revealed a high incidence of somatic mosaicism of *NEMO*.

Submitted May 11, 2011; accepted April 8, 2012. Prepublished online as *Blood* First Edition paper, April 19, 2012; DOI 10.1182/blood-2011-05-354167.

The online version of this article contains a data supplement.

The publication costs of this article were defrayed in part by page charge payment. Therefore, and solely to indicate this fact, this article is hereby marked "advertisement" in accordance with 18 USC section 1734.

Table 1. Clinical and genetic features of XL-EDA-ID patients

Patient	Mutation	Ectodermal dysplasia	Mitogen-induced proliferation	Infections	Complications	Therapy	Sex chromosome chimerism
1	Duplication	+	Reduced	Sepsis (S.P. and P.A.)	Chronic diarrhea	IVIG	100% XY
				Disseminated M.A.C.	Failure to thrive	RFP, CAM, AMK, EB	
				Skin abscess (S.A.)	Small intestinal stenosis	Rifabutin	
				Invasive *Aspergillus*	Lymphedema		
2	Duplication	+	Reduced	Sepsis (*E coli*)	Failure to thrive	IVIG, ST, EB, CAM	99.8% XY 0.2% X
				Disseminated M.S.		Rifabutin, SCT	
3	D311E	−	Normal	Disseminated B.C.G.		IVIG, INH	100% XY
				Sepsis (S.P.)		RFP, SCT	
4	A169P	+	Normal	Meningitis (S.P.)	IBD	IVIG, ST, PSL	99% XY
					Interstitial pneumonia	CyA, MTX, Infliximab	
					Rheumatoid arthritis		
5	L227P	+	Normal	Recurrent pneumonia	IBD	ST, mesalazine	Not done
				Pyogenic coxitis		Infliximab	
				Recurrent otitis media			
6	R182P	+	Not done	Recurrent otitis media	IBD	ST, mesalazine	99.8% XY 0.2% X
				UTI, Recurrent stomatitis			
				Subepidermal abscess			
7	R175P	+	Normal	Recurrent sepsis (S.P.)		IVIG	100% XY
8	Q348X	+	Normal	Disseminated B.C.G.	IBD	IVIG, ST	100% XY
9	R175P	+	Normal	Recurrent pneumonia	IBD	IVIG	100% XY
				Recurrent otitis media		5-aminosalicylic acid	
				Kaposi varicelliform eruption			
10	1167 ins C	+	Normal	Sepsis and Enteritis (E.A)	Failure to thrive	IVIG, SCT	Not done
				Sepsis (C.G.)	Pyloric stenosis, colon polyps		
				UTI (K.P.)			

S.P. indicates *Streptococcus pneumoniae*; P.A., *Pseudomonas aeruginosa*; IVIG, intravascular immunoglobulin infusion; M.A.C., *Mycobacterium avium* complex; S.A., *Staphylococcus aureus*; *E coli*, *Escherichia coli*; ST, trimethoprim-sulfamethoxazole; M.S., *Mycobacterium szulgai*; AMK, amikacin; EB, ethambutol; CAM, clarithromycin; SCT, stem cell transplantation; B.C.G., Bacille de Calmette et Guerin; INH, isoniazid; RFP, rifampicin; IBD, inflammatory bowel disease; PSL, prednisolone; CyA, cyclosporine A; MTX, methotrexate; UTI, urinary tract infection; E.A., *Enterobacter aerogenes*; C.G., *Candida glabrata*; and K.P., *Klebsiella* pneumonia.

Methods

Informed consent

Informed consent was obtained from the patients and their families following the Declaration of Helsinki according to the protocol of the Internal Review Board of Kyoto University, which approved this study.

Patients

Patient 1 was an XL-EDA-ID patient with a duplication mutation of the *NEMO* gene spanning intron 3 to exon 6. This patient has been reported previously[17] and died from an *Aspergillus* infection at the age of 4. Patient 2, born at term, was the younger brother of patient 1. This patient was also diagnosed as XL-EDA-ID with the same duplication mutation as patient 1 by genetic study. He received trimethoprim-sulfamethoxazole prophylaxis and a monthly infusion of immunoglobulin from the age of 1 month. The patient maintained good health and had a body weight of 7899*g* at 6 months when he started to fail to thrive. Except for poor weight gain, patient 2 appeared active with a good appetite, negative C-reactive protein, normal white blood cell counts, and no apparent symptoms. At 19 months of age, *Mycobacterium szulgai* was detected by venous blood culture, and the patient was treated with multidrug regimens including ethambutol, rifabutin, and clarithromycin based on the treatment of systemic *Mycobacterium avium* complex infection. The patient responded well to the treatment and his weight increased from 7830*g* to 9165*g* within a month after the treatment was initiated. Patient 2 received an unrelated cord blood cell transplantation at 26 months of age, containing 8.5×10^7 nucleated cells/kg (4.4×10^5 $CD34^+$ cells/kg), which was matched at 5 of 8 loci: mismatches occurred at 1 HLA-B and 1 HLA-C allele (according to serology), and at 1 HLA-A, 1 HLA-B, and 1 HLA-C allele (according to DNA typing). The preconditioning regimen consisted of fludarabine (30 mg/m^2/d) on days −7 to −3, melphalan (70 mg/m^2/d) on days −6 to −5, and rabbit anti-thymocyte globulin (2.5 mg/kg/d) on days −6 to −2. At first, Tacrolimus (0.024 mg/kg/d) was used to prevent GVHD, but this was switched to cyclosporin A (3 mg/kg/d) on day 9 because of drug-induced encephalopathy. Neutrophil ($> 0.5 \times 10^9$/L) and platelet ($> 50 \times 10^9$/L) engraftment were examined on days 13 and 40, respectively. Although $CD19^+$ cells (2042/μL, 94% donor chimerism), $CD56^+$ cells (242/μL, 97% donor chimerism), and monocytes (557/μL, 69% donor chimerism) were successfully generated, $CD3^+$ cells were not detected in the peripheral blood by day 54. The patient suffered from septic shock and died on day 60. Patients 3 to 10 were XL-EDA-ID patients recruited nationwide in Japan. Clinical details of patients 3, 4, and 10 have been reported previously.[18-20] These patients had clinical phenotypes characteristic of XL-EDA-ID such as ectodermal dysplasia, innate and/or acquired immunity defects, and susceptibility to pyogenic bacteria and *Mycobacterium* infection. Every patient had a mutation in the *NEMO* gene that caused reduced NF-κB activation in a NEMO reconstitution assay, as described in "Proliferation of $NEMO^{normal}$ and $NEMO^{low}$ T cells." Patient profiles are listed in Table 1.

Flow cytometric analysis

NEMO intracellular staining was performed as previously described.[17] The cells were stained for the following lineage markers before staining for NEMO: CD4, CD8, CD14, CD15, CD19, CD56, CD45RA (BD Biosciences/BD Pharmingen), and CCR7 (R&D Systems Inc). Intracellular staining of human IFN-γ, TNF-α, and NEMO was performed as previously described.[18] The stained cells were collected using a FACSCalibur flow cytometer (BD Biosciences) and analyzed using the FlowJo software (TreeStar).

Reporter assay

Wild-type and mutant *NEMO* cDNAs were generated from a healthy volunteer and the recruited XL-EDA-ID patients by RT-PCR; the cDNAs were subcloned into the p3xFLAG-CMV14 vector (Sigma-Aldrich). NEMO null rat fibroblast cells (kindly provided by Dr S. Yamaoka, Department of Molecular Virology, Graduate School of Medicine, Tokyo Medical and Dental University, Tokyo, Japan) were plated at a density of

3×10^4 cells/well in a 24-well culture dish and were transfected with 40 ng of NF-κB reporter plasmid (pNF-κB-Luc; BD Biosciences/BD Clontech), 2 ng of *NEMO* mutant expression construct, 10 ng of internal control for the normalization of transfection efficiency (pRL-TK; Toyo Ink), and 148 ng of mock vector using FuGENE HD Transfection Reagent (TOYO-B-Net) according to the manufacturer's protocol. Twelve hours after transfection, the cells were stimulated with 15 ng/mL lipopolysaccharide (LPS; Sigma-Aldrich) for 4 hours and the NF-κB activity was measured using the PicaGene Dual SeaPansy assay kit (TOYO-B-Net). Experiments were performed in triplicate and firefly luciferase activity was normalized to *Renilla* luciferase activity.

Subcloning analysis of cDNA

Cell sorting of the various cell lineages was performed by FACSVantage (BD Biosciences). The purity of each lineage was > 95%. The cDNA from sorted cells was purified and reverse transcribed by Super Script III (Invitrogen) with random hexamers and amplified by the proofreading PCR enzyme KOD, as previously described.[17,21] The PCR primers used were NEMO2 (5′-AGAGACGAAGGAGCACAAAGCTGCCTTGAG-3′) and NEMO3 (5′-ACTGCAGGGACAATGGTGGGTGCATCTGTC-3′). The PCR products were subcloned using a TA cloning kit (Invitrogen) and sequenced by ABI 3130xl Genetic analyzer (Applied Biosystems). To determine whether additional mutations occurred in revertant subclones that had wild-type sequence in the original mutation site, the entire coding region of the *NEMO* gene was sequenced and an additional mutation was considered present when the same mutation was detected in multiple subclones.

Allele-specific PCR

The mRNA purified from sorted T cells and monocytes was reverse-transcribed by SuperScript III (Invitrogen) with the gene-specific primer NEMO2 and amplified by the proofreading PCR enzyme KOD (Toyobo) using the primers NEMO3 and NEMO 4 (5′-TGTGGACACGCAGTGAAACGTGGTCTGGAG-3′). The PCR products were used as templates for allele-specific PCRs with Ex Taq polymerase (Takara Bio). Mutant and wild-type *NEMO* DNA was generated from each NEMO expression plasmid, mixed at graded ratios, and used as controls. PCR conditions and primer sequences are listed in supplemental Table 1 (available on the *Blood* Web site; see the Supplemental Materials link at the top of the online article).

Proliferation of NEMO^{normal} and NEMO^{low} T cells

To obtain PHA-induced T-cell blasts, PBMCs were stimulated with PHA (1:100; Invitrogen) and cultured in RPMI 1640 supplemented with 5% FCS and recombinant human IL-2 (50 IU/mL; kindly provided by Takeda Pharmaceutical Company) at 37°C for 7 days. Subcloning analysis of the cDNA obtained from the T-cell blasts was performed as described in "Subcloning analysis of cDNA."

Results

Reversion mosaicism of NEMO occurred in siblings with similar immunologic phenotypes

We previously reported patient 1 with a duplication mutation of the *NEMO* gene spanning intron 3 to exon 6, who was diagnosed as XL-EDA-ID at 1 year of age after suffering from recurrent infections.[17] At first, genetic diagnosis of the patient was difficult because the expression of aberrant *NEMO* mRNA was masked by the expression of normal *NEMO* mRNA by the revertant cells. Flow cytometric analysis of intracellular NEMO expression revealed cells with normal (NEMO^{normal}) and reduced (NEMO^{low}) levels of NEMO expression, indicating the presence of reversion mosaicism of the *NEMO* gene, and further analysis revealed that the *NEMO* mutation was disease-causing. PCR across the mutated region and sequencing of the PCR products revealed a duplication extending from intron 3 to exon 6, which was confirmed by Southern blot analysis. Additional copy number analysis of the *NEMO* gene of patient 1 and his mother excluded the possibility of a complex chromosomal aberration such as multiple duplication of the *NEMO* gene (supplemental Figure 1). Furthermore, polymorphism analysis using variable number tandem repeats on NEMO^{normal} and NEMO^{low} cells from patient 1 revealed that these cells were derived from the same origin (supplemental Table 2), indicating that the *NEMO* gene mosaicism was less likely because of amalgamation. The genomic analysis of the NEMO^{normal} cells revealed a complete reversion of the *NEMO* gene with no additional mutations. The clinical phenotype of patient 1 was combined immunodeficiency with a reduced number of T cells and mitogen-induced proliferation (Tables 2-3). We previously determined that reduced NEMO expression in the mutant T cells caused impairment of T-cell development and mitogen-induced proliferation.

Patient 2, the younger brother of patient 1, was diagnosed as XL-EDA-ID with the same duplication mutation as his brother. Flow cytometric analysis of intracellular NEMO expression performed at diagnosis showed that most of his PBMCs had reduced NEMO expression (Figure 1A). At 2 months of age, when most of the T cells were NEMO^{low}, absolute counts of the patient's T cells and the mitogen-induced proliferation of the patient's PBMCs were comparable with those of the healthy controls (Figure 1A-B; Table 2). These findings indicated that the *NEMO* mutation had no effect on T-cell development and mitogen-induced proliferation during early infancy in patient 2.

NEMO^{normal} T cells gradually increased as patient 2 grew older, while the absolute count of NEMO^{low} T cells decreased (Figure 1A-B). Accordingly, normal full-length *NEMO* cDNA, which had been undetectable in cord blood, was detectable in the patient's peripheral blood at 12 months of age. However, while NEMO^{normal} T cells were increasing, mitogen-induced T-cell proliferation started to decrease (Table 3), and the patient started to show poor weight gain from 6 months of age. When patient 2 was 17 months old, a blood culture revealed an *M szulgai* bacteremia. At this time, the absolute count of NEMO^{normal} T cells peaked, and NEMO^{low} T cells were at a minimum. He began to gain weight after anti-*Mycobacterium* medication was initiated, although NEMO^{normal} T cells started to decrease and NEMO^{low} T cells began to increase (Figure 1B). When the patient was 23 months old, mitogen-induced T-cell proliferation was still low and a roughly equal number of NEMO^{low} and NEMO^{normal} T cells were detected (Table 3). Overall, as patient 2 grew older, NEMO^{normal} T cells increased as the total number of T cells and the mitogen-induced T-cell proliferation decreased, similar to what had occurred in patient 1 at a similar age.

Various analyses were performed to compare the immunologic phenotype of NEMO^{low} and NEMO^{normal} T cells in detail. Both NEMO^{normal} and NEMO^{low} CD4$^+$ T cells carried a diverse Vβ repertoire, but CD8$^+$ T cells had a skewed Vβ repertoire regardless of NEMO expression level (Figure 1C). Surface marker analysis revealed that most of the NEMO^{normal} T cells were CD45RA$^-$/CCR7$^-$ and most of the NEMO^{low} T cells were CD45RA$^+$/CCR7$^+$ (Figure 1D). The NEMO^{normal} T cells produced similar amounts of IFN-γ and TNF-α as healthy control cells, while the production of these cytokines were reduced in NEMO^{low} T cells (Figure 1E-F). Taken together, these data implied that the immunologic phenotype of T cells from patient 2 converged with that of patient 1 as patient 2 grew older.

Table 2. Surface marker analysis of peripheral mononuclear cells of patients 1 and 2

	Patient 1	Patient 2		Healthy controls
Age at analysis	2 y	2 mo	19 mo	
CD3	1503	2366	1014	2997 ± 1751
CD4	292	1583	374	1683 ± 874
CD8	1160	783	547	1114 ± 976
TCRαβ	1386	2295	439	2620 ± 1612
TCRγδ	109	74	574	343 ± 177
$CD4^+CD45RA$	58	1336	105	1471 ± 890
$CD4^+CD45RO$	263	307	266	497 ± 189
$CD8^+CD45RA$	1178	783	297	1083 ± 1078
$CD8^+CD45RO$	361	21	250	385 ± 442
$CD4^+CD25$	80	427	93	210 ± 99
CD19	1200	941	1543	1252 ± 1145
CD20	1189	931	1536	1125 ± 837
$CD19^+$Sm-IgG	7	18	17	54 ± 21
$CD19^+$Sm-IgA	15	4	14	18 ± 14
$CD19^+$Sm-IgM	1171	910	1505	1057 ± 881
$CD19^+$Sm-IgD	1171	906	1495	1052 ± 884
CD16	912	176	24	287 ± 200
CD56	908	176	24	306 ± 207

Surface markers expressed by XL-EDA-ID patients' PBMCs are shown as absolute counts per microliter of peripheral blood. Healthy control values are based on children aged 1 to 6 years and are shown as the mean ± SD.

Sm indicates the surface membrane.

High incidence of somatic mosaicism of the *NEMO* gene in XL-EDA-ID patients

It is worth noting that somatic reversion mosaicism of the *NEMO* gene occurred in both of the 2 XL-EDA-ID siblings carrying a duplication mutation. To determine whether a high frequency of reversion is a specific event for this type of *NEMO* duplication mutation[22-25] or if the reversion of the *NEMO* gene occurs commonly in XL-EDA-ID patients, we recruited an additional 8 XL-EDA-ID patients from throughout Japan (Table 1) and analyzed the presence of *NEMO* reversion. These patients had various combinations of clinical phenotypes characteristic of XL-EDA-ID such as ectodermal dysplasia, innate and acquired immunity defects, and susceptibility to pyogenic bacteria and *Mycobacterium* infections. Every patient had a mutation of the *NEMO* gene with reduced NF-κB activation potential, as evaluated in a NEMO reconstitution assay (Figure 2).

Among the 8 patients, only patient 3 had a large proportion of $NEMO^{low}$ cells by flow cytometric analysis. The majority of patient 3's PBMCs were $NEMO^{low}$, whereas 10% of the patient's $CD8^+$ cells were $NEMO^{normal}$ (Figure 3A). This patient was identified as carrying the D311E mutation. Because missense mutations of the *NEMO* gene often do not result in the reduced expression of NEMO protein, subcloning and sequencing analysis was performed on the *NEMO* cDNA isolated from the remaining patients, and 6 of the 7 patients had normal *NEMO* subclones (Table 3). Expansion of maternal cells after fetomaternal transfusion was ruled out in these patients by FISH analysis with X and Y probes (Table 1).

Additional genetic analysis of the entire coding region of the *NEMO* gene was performed on $NEMO^{normal}$ cells from patient 3 and on reverted subclones from the other patients, except for patient 10 who had already received stem cell transplantation. The *NEMO* gene in these samples had reverted to wild-type with no additional mutations (Figure 3B and data not shown). To specifically determine in which cell lineages the reversion occurred, subcloning and sequencing analysis of cDNA in various cell lineages was performed. This analysis revealed that all the revertant cells were of the T-cell lineage and that no reversion occurred in monocytes and very little occurred in B cells (Table 4). Allele-specific PCR confirmed that reversion occurred in T cells but not in monocytes (Figure 4).

Selective advantage of $NEMO^{normal}$ cells in XL-EDA-ID carriers

The high frequency of somatic mosaicism in T cells of XL-EDA-ID patients indicated a strong selective advantage of wild-type NEMO T cells over T cells carrying mutant NEMO. To confirm this hypothesis, *NEMO* cDNA analysis was performed on various cell lineages from the mothers of the patients who are heterozygous for *NEMO* mutation and thus have mosaicism

Table 3. Immunologic analysis of patients 1 and 2

	Patient 1	Patient 2 (treated with IVIG)	
Age at analysis, mo	9	9	20
Serum immunoglobulin levels, g/L (control)			
IgG	10.63 (4.51-10.46)	8.44 (4.51-10.46)	10.37 (7.15-9.07)
IgA	1.36 (0.14-0.64)	1.88 (0.14-0.64)	3.93 (0.22-1.44)
IgM	0.4 (0.33-1.00)	0.17 (0.33-1.00)	0.20 (0.34-1.28)
Age at analysis	2 y	2 mo	23 mo
T-cell proliferation, SI (control)	9.3 (206.9 ± 142.5)	55.3 (64.8 ± 8.1)	7.2 (89.4 ± 31.2)

Control values of serum immunoglobulin levels are based on children aged either 7 to 9 months or 1 to 2 years and are shown as the mean ± SD. The T-cell proliferation assay was performed as described previously[17] with at least three healthy adults as controls.

SI indicates stimulation index; and IVIG, 2.5 g of monthly IV immune globulin infusion.

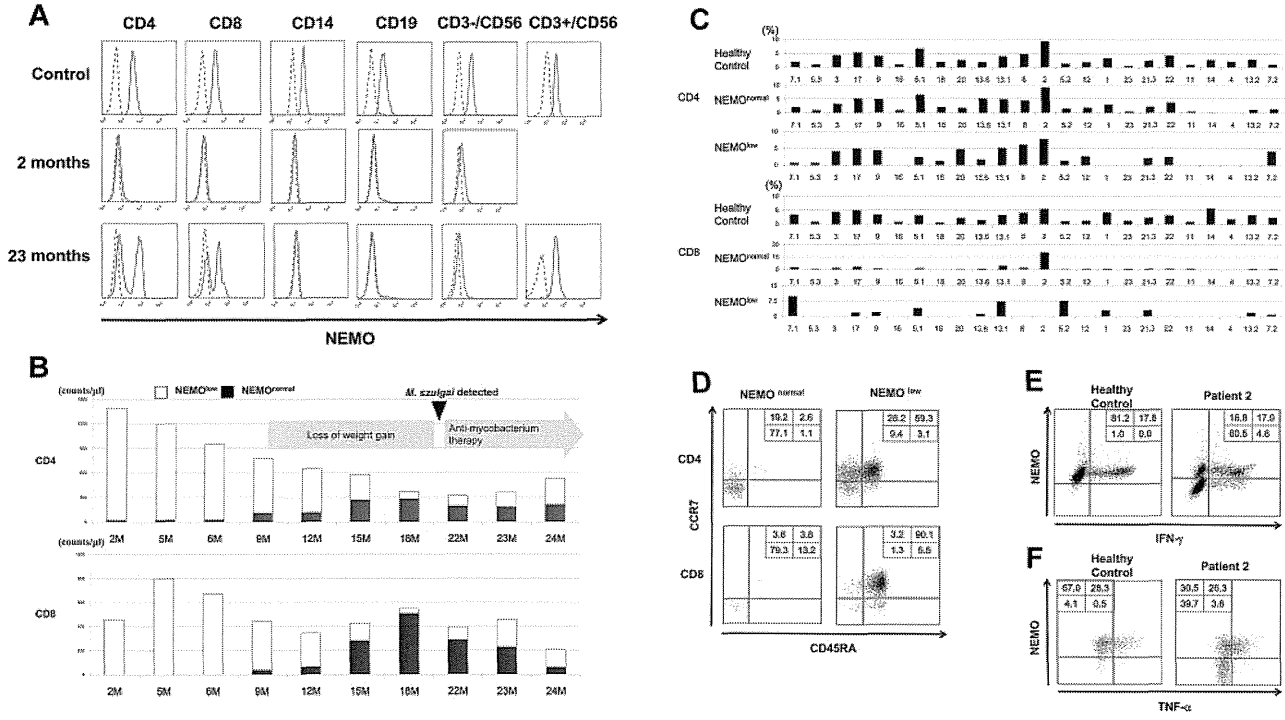

Figure 1. Identification and characterization of *NEMO* revertant T cells in patient 2. (A) Intracellular expression of NEMO in various PBMC lineages from a healthy adult control and patient 2 were evaluated by flow cytometry. For the patient, results of the analyses performed at 2 months and 23 months are shown. Solid lines indicate staining with the anti-NEMO mAb, and dotted lines indicate the isotype control. (B) Time-course variations in the absolute count of $NEMO^{normal}$ and $NEMO^{low}$ T cells in patient 2. M indicates age in months. (C) TCR-Vβ repertoire analysis of the patient's $CD4^+$ and $CD8^+$ T cells. PBMCs from the patient and a healthy adult control were stained for the TCR-Vβ panel, CD4, CD8, and NEMO, and analyzed by flow cytometry. (D) Phenotype analysis of T cells in patient 2. PBMCs from the patient and a control were stained for the expression of NEMO, CCR7, CD45RA, and CD4 or CD8. Data shown were gated on $NEMO^{normal}$ or $NEMO^{low}$ $CD4^+$ or $CD8^+$ cells. (E-F) Cytokine production from $NEMO^{normal}$ and $NEMO^{low}$ T cells. PBMCs from the patient and a control were stimulated with PMA and ionomycin for 6 hours and stained for intracellular (E) IFN-γ or (F) TNF-α along with NEMO. Cells shown are gated on the $CD3^+$ population.

because of X-chromosome inactivation. This analysis assumes that the percentage of cDNA for wild-type *NEMO* reflects the percentage of cells expressing wild-type NEMO. A high proportion of wild-type *NEMO* cDNA was observed in T cells from the mothers of patients 1/2, 3, 8, and 10, although wild-type *NEMO* cDNA was not predominant in T cells from the mother of patient 4 (Table 5).

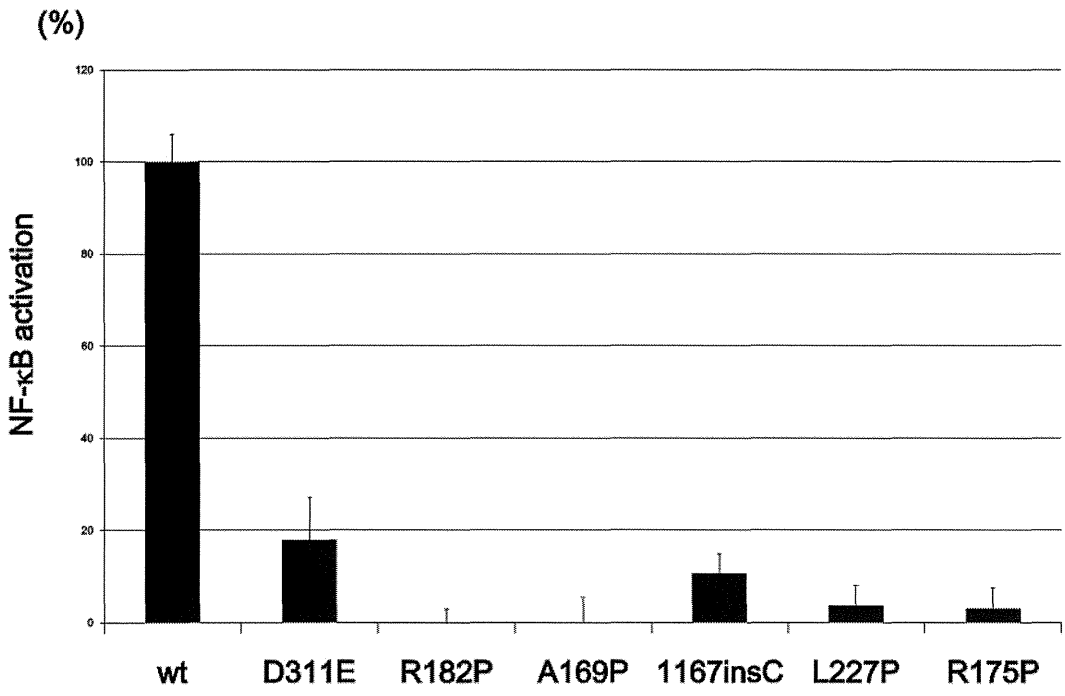

Figure 2. NF-κB transactivation by NEMO mutants from the XL-EDA-ID patients. NF-κB transactivation induced by NEMO mutants in the XL-EDA-ID patients. Mock vectors and wild-type (wt) NEMO were used as controls. The NF-κB activation index of NEMO variants were calculated as (NF-κB activation by each NEMO variant − NF-κB activation of the mock vector)/(NF-κB activation by wild-type NEMO − NF-κB activation of the mock vector). The data shown are the mean ± SD of triplicate wells and are representative of 3 independent experiments with similar results.

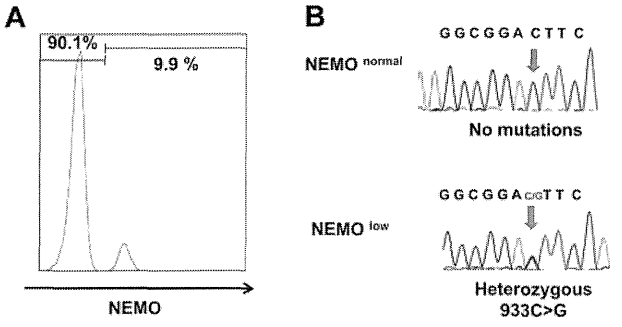

Figure 3. *NEMO* revertant T cells in patient 3. (A) Intracellular expression of NEMO in $CD8^+$ cells from patient 3. (B) Sequencing chromatograms of DNA from $NEMO^{normal}$ or $NEMO^{low}$ $CD8^+$ cells of patient 3. Arrows indicate the mutated base position at c. 931.

Similarly, there was an apparent high proportion of wild-type *NEMO* cDNA in monocytes and B cells from the mothers of patients 1/2, 8, and 10 (Table 5). These findings suggested a general selective advantage of $NEMO^{normal}$ cells over $NEMO^{low}$ cells in vivo, especially in T cells.

Proliferation capacity of $NEMO^{normal}$ and $NEMO^{low}$ T cells

T-cell proliferation stimulated by mitogens such as PHA is usually not reduced in XL-EDA-ID patients. However, the emergence of $NEMO^{normal}$ cells coincided with a reduction in mitogen-induced proliferation in patient 2. To further determine the effect of $NEMO^{normal}$ cells on mitogen-induced proliferation of peripheral T cells, the proportions of T cells carrying the wild-type and mutant were examined before and after PHA stimulation in XL-EDA-ID patients and their mothers (Table 6). In patients 2, 4, and 8, the percentage of the $NEMO^{normal}$ cells decreased after PHA stimulation, while $NEMO^{normal}$ cells prevailed in patient 9. In the mothers of patient 4 and 10, the percentage of $NEMO^{normal}$ cells increased after PHA stimulation, while the percentage of the $NEMO^{normal}$ cells decreased in the mother of patient 3. These results indicated that the NEMO mutation does not directly affect the mitogen-induced proliferation capacity of T cells and factors other than the *NEMO* genotype determine the proliferation capacity of $NEMO^{normal}$ and $NEMO^{low}$ T cells.

Discussion

Somatic reversion mosaicism has been described in several disorders affecting the hematopoietic system, the liver, and the skin.[23,26] Reports of somatic reversion cases have been particularly abundant in patients with immunodeficiency diseases, including Wiskott-Aldrich syndrome (WAS)[27] and SCID, which occur because of mutations in the interleukin receptor common γ chain,[28] CD3ζ,[29] *RAG-1*[30], and *ADA* genes.[31] Patients with somatic reversion mosaicism may present with significantly milder clinical phenotypes compared with nonrevertant patients with the same germline mutation, although this is not always the case.[26] One common feature in most cases where the somatic reversion mosaicism has been observed is a strong in vivo selective advantage of the revertant cells that express the wild-type gene product. One of the most intensively investigated diseases associated with somatic reversion mosaicism is WAS.[32-34] A report showed that up to 11% of WAS patients have presented with somatic reversion mosaicism.[33]

In our investigation, 9 of 10 XL-EDA-ID patients presented with somatic mosaicism. Two of the 9 were cases of reversion from a duplication mutation, while the others exhibited true back-reversion from a substitution or insertion mutation. This finding calls for caution when diagnosing XL-EDA-ID patients. Because the existence of a *NEMO* pseudogene makes it difficult to perform genetic analysis using genomic DNA, diagnosis of the disease is often confirmed by sequencing analysis of *NEMO* cDNA, and the presence of somatic mosaicism can cause misdiagnosis of XL-EDA-ID patients either when $NEMO^{normal}$ cells make up the majority of the patients' PBMCs or when the cDNA of the mutated *NEMO* gene cannot be amplified by PCR.[17] In fact, mutated *NEMO* cDNA could not be amplified from the PBMCs of patient 2 even when $NEMO^{normal}$ cells were absent (during early infancy), and only wild-type *NEMO* cDNA was amplified after the appearance of $NEMO^{normal}$ cells (data not shown), probably because of the instability of the mutated *NEMO* mRNA. Flow cytometric analysis of intracellular NEMO protein is of help in identifying the $NEMO^{low}$ cells in some patients, but the technique is not applicable when the *NEMO* mutation does not cause reduced expression of NEMO protein. Thus, some cases of XL-EDA-ID patients with reversion may be difficult to diagnose.

The high frequency of somatic mosaicism observed in XL-EDA-ID patients indicates a strong in vivo selective advantage for $NEMO^{normal}$ cells, which express the wild-type gene product. Patient 2 presented with a high mutant T-cell count at birth that gradually decreased over time (Figure 1B). This finding indicates that wild-type NEMO expression is critical for the survival of certain cell lineages, including T cells, after birth. On the other hand, no $NEMO^{normal}$ monocytes and very few $NEMO^{normal}$ B cells were detected in the recruited XL-EDA-ID patients (Table 4). This specific feature is similar to other somatic reversion mosaicism seen in primary immunodeficiency patients[26] and indicates that the expression of NEMO is less critical for the survival of monocytes or B cells compared with that of T cells. There is also an apparent

Table 4. Analysis of *NEMO* gene mosaicism in various cell lineages for each patient

Patient	Mutation	Age at analysis	CD4, % (proportion)	CD8, % (proportion)	CD14, % (proportion)	CD19, % (proportion)
1	Duplication	2 y	90	100	0	4.0
2	Duplication	15 mo	45	66	0	4.0
3	D311E	3 y	2.4	9.9	0	1.2
4	A169P	12 y	0 (0/19)	24 (9/37)	0 (0/19)	0 (0/47)
5	L227P	3 y	0 (0/25)	0 (0/35)	0 (0/30)	0 (0/25)
6	R182P	4 y	18 (5/28)	17 (9/52)	0 (0/27)	0 (0/33)
7	R175P	6 y	0.4 (1/25)	39 (11/28)	0 (0/28)	0 (0/25)
8	Q348X	8 y	38 (6/16)	47 (9/19)	0 (0/33)	0 (0/25)
9	R175P	15 y	30 (9/30)	36 (12/33)	0 (0/23)	0 (0/14)
10	1167 ins C	9 mo		PBMC 9.3 (4/43)		

For patients 1 to 3, data represent the percentages of $NEMO^{normal}$ cells in each lineage, as assessed by flow cytometry. For patients 4 to 10, the ratio indicates the number of wild-type NEMO clones in various cell lineages as compared with the total number of clones analyzed, based on subcloning and sequencing analysis.